# Synoptic Regulation of the 3 May 1999 Tornado Outbreak

PAUL J. ROEBBER

*Atmospheric Science Group, Department of Mathematical Sciences, University of Wisconsin—Milwaukee, Milwaukee, Wisconsin*

DAVID M. SCHULTZ AND ROMUALDO ROMERO*

*NOAA/OAR/National Severe Storms Laboratory, Norman, Oklahoma*

(Manuscript received 23 February 2001, in final form 10 December 2001)

ABSTRACT

Despite the relatively successful long-lead-time forecasts of the storms during the 3 May 1999 tornadic outbreak in Oklahoma and Kansas, forecasters were unable to predict with confidence details concerning convective initiation and convective mode. The forecasters identified three synoptic processes they were monitoring for clues as to how the event would unfold. These elements were (a) the absence of strong surface convergence along a dryline in western Oklahoma and the Texas Panhandle, (b) the presence of a cirrus shield that was hypothesized to limit surface heating, and (c) the arrival into Oklahoma of an upper-level wind speed maximum [associated with the so-called southern potential vorticity (PV) anomaly] that was responsible for favorable synoptic-scale ascent and the cirrus shield. The Pennsylvania State University–National Center for Atmospheric Research Fifth-Generation Mesoscale Model (MM5), nested down to 2-km horizontal grid spacing, is used in forecast mode [using the data from the National Centers for Environmental Prediction Aviation (AVN) run of the Global Spectral Model to provide initial and lateral boundary conditions] to explore the sensitivity of the outbreak to these features. A 30-h control simulation is compared with the available observations and captures important qualitative characteristics of the event, including convective initiation east of the dryline and organization of mesoscale convective systems into long-lived, long-track supercells. Additional simulations in which the initial strength of the southern PV anomaly is altered suggest that synoptic regulation of the 3 May 1999 event was imposed by the effects of the southern PV anomaly. The model results indicate that 1) convective initiation in the weakly forced environment was achieved through modification of the existing cap through both surface heating and synoptic-scale ascent associated with the southern PV anomaly; 2) supercellular organization was supported regardless of the strength of the southern PV anomaly, although weak-to-moderate forcing from this feature was most conducive to the production of long-lived supercells and strong forcing resulted in a trend toward linear mesoscale convective systems; and 3) the cirrus shield was important in limiting development of convection and reducing competition between storms. The implications of these results for the use of high-resolution models in operational forecasting environments are discussed. The model information provides potentially useful information to forecasters following the scientific forecast process, most particularly by assisting in the revision of conceptual ideas about the evolution of the outbreak. Substantial obstacles to operational implementation of such tools remain, however, including lack of model context (e.g., information concerning model biases), insufficient real-time observations to assess effectively model prediction details from the synoptic to the mesoscale, inconsistent forecaster education, and inadequate technology to support rapid scientific discovery in an operational setting.

## 1. Introduction

On 3 May 1999, parts of central and northern Oklahoma and southern Kansas were devastated by 10 supercells that produced a total of 66 tornadoes (NCDC 1999; Speheger et al. 2002). This outbreak was comparable to past major outbreaks as measured by the number of strong to violent tornadoes and the nearly $1 billion in damages (Thompson and Edwards 2000, hereinafter TE; Brooks and Doswell 2001). Despite this destruction, there were only 46 fatalities (Brooks and Doswell 2002). In contrast, the review of historical damage and fatality data from major U.S. tornadic outbreaks by Doswell et al. (1999) and Brooks and Doswell (2002) suggests 500 or more fatalities for an event of the magnitude of 3 May 1999 in the absence of mitigation efforts [the National Weather Service (NWS) outlook/watch/warning system and societal advances in communications and construction]. One factor that worked to reduce potential casualties on 3 May was that forecasters

* Current affiliation: Grup de Meteorologia, Departament de Física, Universitat de les Illes Balears, Palma de Mallorca, Spain.

*Corresponding author address:* Paul J. Roebber, Dept. of Mathematical Sciences, University of Wisconsin—Milwaukee, 3200 N. Cramer Ave., Milwaukee, WI 53211.
E-mail: roebber@uwm.edu

TABLE 1. Time sequence of selected statements concerning convective initiation from forecast discussions of the NWS office at Norman (OUN), OK, and convective outlooks and mesoscale discussions from the SPC issued on 3 May 1999. The time is UTC.

| Time (office) | Forecaster statements concerning convective initiation |
|---|---|
| 0555 (SPC) | Primary convective potential across much of the SRN plains should be through the evening/overnight as upper system lifts EWD ... and low level convergence increases as surface trough/dry line moves into central OK/TX. |
| 0836 (OUN) | Dryline currently retreating slowly into TX Panhandle, but is expected to move back E into western OK by late afternoon. Low clouds should break up by midday, allowing sufficient heating and destabilization for scattered T-storms to develop along and possibly ahead of dryline late this afternoon. |
| 1246 (SPC) | Expect greatest convective threat after about 23Z ... when large-scale ascent associated with AZ shortwave trough begins to impinge upon dryline region. Subsidence associated with foregoing shortwave ridge should help to remove both cloud cover and convective threat in the meantime...while aiding diabatic surface heating. |
| 1549 (OUN) | With the upper wave over western AZ this morning and convergence along the dryline rather weak, no thunderstorms are expected until very late this afternoon or later. |
| 1615 (SPC) | As short wave approaches WRN OK/TX border ... lifting will deepen near/along dry line with thunderstorms increasing as they move EWD into instability axis. |
| 1957 (OUN) | A dry line near the TX/OK border will slowly work its way east for the first part of this evening. As storms become organized along the dry line later this evening they will move eastward across the state overnight. |
| 2023 (SPC) | Convergence on the dryline is not strong and a cirrus shield over the TX Panhandle/NW TX/WRN OK should limit additional surface heating ... but visible/radar imagery has shown the first attempts at TCU over far NW TX as of 20Z within a break in the cirrus. |
| 2153 (SPC) | Low-level convergence along dry line is still quite weak. |

were able to capitalize on the storms' general motion from sparsely populated regions into population centers, resulting in substantial lead times for the majority of those affected.

Despite this success, neither NWS forecasters in Norman, Oklahoma (OUN), nor the convective storm specialists of the Storm Prediction Center (SPC) were able to predict with confidence details concerning convective initiation (Table 1) and convective mode (Table 2) (Edwards et al. 2002, hereinafter E02). Statements from both OUN and SPC forecast products indicate the difficulty this situation posed (Tables 1 and 2).

As early as 0728 UTC 2 May, the SPC forecaster issuing the day-2 convective outlook (not shown) recognized the importance of surface heating and an upper-level short-wave trough/jet streak to destabilizing the environment over the southern plains: ''Combination of surface heating and increasing upper divergence associated with approaching upper disturbance will create an increasingly favorable environment for severe thunderstorms over parts of west Texas and southwestern Oklahoma Monday afternoon.'' However, ''large-scale surface features [e.g., dryline] will remain fairly ill-defined.''

By 1246 UTC 3 May, the day-1 convective outlook provided more details into the thinking of SPC forecasters (Table 1): ''Expect greatest convective threat after about 23Z . . . when large-scale ascent associated with Arizona shortwave trough begins to impinge upon dryline region. . . . Upper-level flow . . . should help to

TABLE 2. Time sequence of selected statements concerning convective mode from forecast discussions of the NWS office at OUN, and convective outlooks and mesoscale discussions from the SPC issued on 3 May 1999.

| Time (office) | Forecaster statements concerning convective mode |
|---|---|
| 0555 (SPC) | Isolated thunderstorms should begin developing toward 00Z over far WRN OK/NWRN TX within very unstable air mass. Initial activity should be supercellular ... though activity will likely evolve into a squall line later in the evening across central/ERN KS ... OK ... central/NERN TX. |
| 0836 (OUN) | Storms likely will evolve into a linear or quasi-linear MCS. Main severe threat, including potential for tornadic supercells, will be this afternoon and evening before convection evolves into a more organized mesoscale system tonight. |
| 1246 (SPC) | Upper level flow is expected to back during late afternoon and evening as AZ shortwave trough approaches. This should help to trend storm evolution toward HP then linear ... brief window of tornado potential may exist with a few storms between about an hour after initiation ... and fully outflow-dominant HP transition. However ... main threat should be large hail first few hours after initiation ... transitioning to damaging wind. |
| 1615 (SPC) | 50 kt mid level SWLY flow spreading over low level jet axis will provide sufficient shear for a few strong or violent tornadic supercells. |
| 2023 (SPC) | Mid level flow and vertical shear will increase over NW TX and WRN OK through late afternoon ... with an increasing threat of supercells near the dryline from 00-03Z. |
| 2049 (SPC) | Storm relative inflow is forcast to increase this evening across OK with 50 kt forecast into the dry line after 00Z ... is expected to enhance helicity in the vicinity of the squall line. Thus ... isolated tornadoes are expected ... with the main threat being large hail. |
| 2153 (SPC) | Convergence along dry line will strengthen ... supporting supercell development along dry line through much of western Texas between 04/00Z and 04/03Z. Activity will quickly become severe ... with strong shear profiles supportive of tornadoes ... in addition to very large hail and damaging wind gusts. |

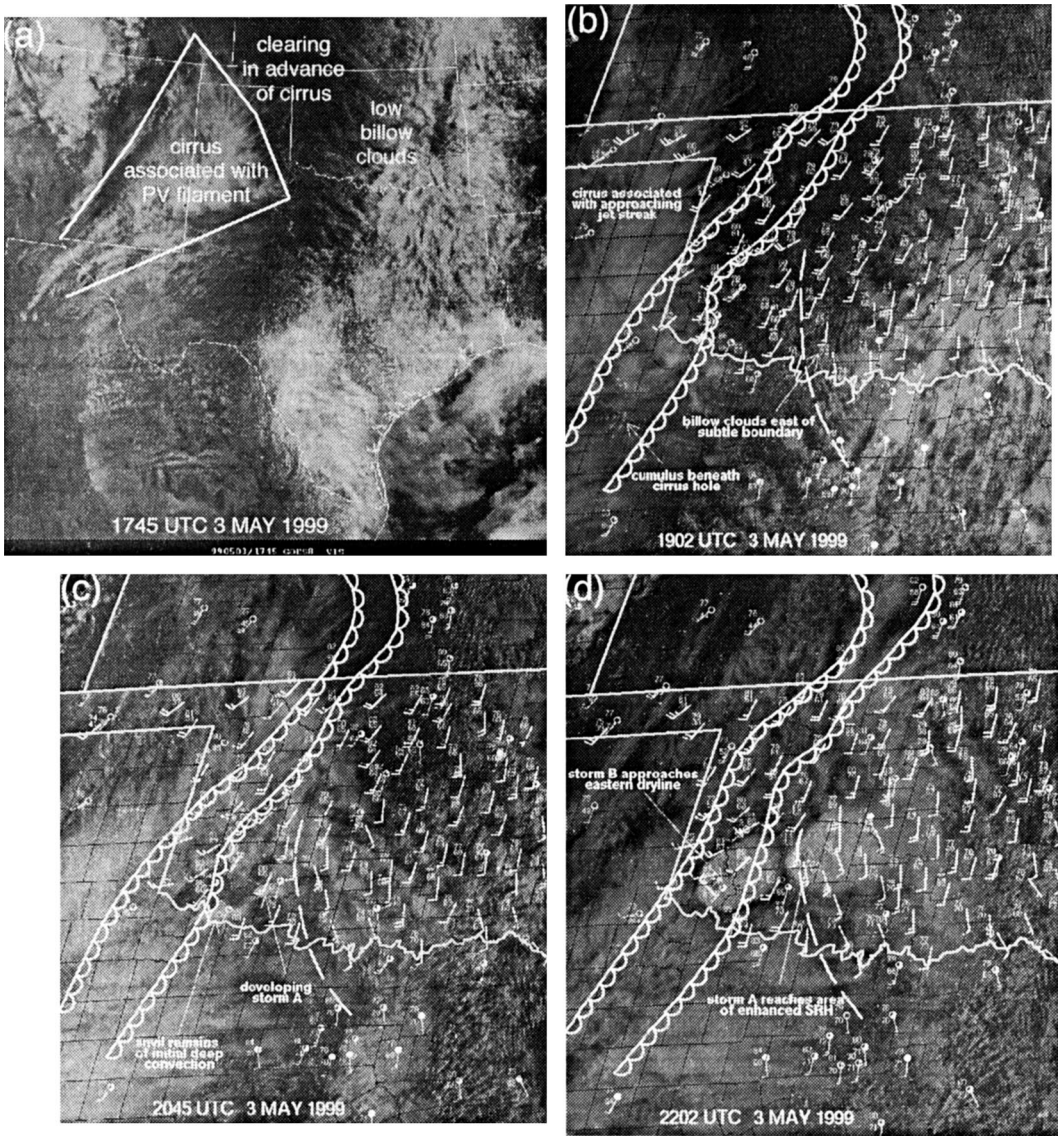


FIG. 1. Series of *GOES-8* visible satellite images at (a) 2- and (b)–(d) 1-km resolution. Associated surface station data plots are in (b), (c), and (d). Annotations denote cloud features, with the surface dryline positions marked by the open scalloped lines and a subtle confluence zone across southern OK marked by a dashed line. Solid polygon in (a) represents outer boundary of cirrus shield. Plotted mesonet observations are within 2 min of each respective satellite image, whereas standard surface observations are from within the hour before each image: (a) 1745, (b) 1902, (c) 2045, and (d) 2202 UTC 3 May 1999. Panels (b), (c), and (d) are from Thompson and Edwards (2000), their Fig. 8.

trend storm evolution toward HP [high-precipitation supercells] then linear [mesoscale convective system]. . . . Line of strong-severe thunderstorms is expected to form from afternoon/early evening development.''

By 1800 UTC 3 May, however, exchanges during the daily National Severe Storms Laboratory–SPC map discussion, later codified in a 2023 UTC mesoscale discussion (Tables 1 and 2), raised questions about three factors: the intensity of the dryline, the degree of upper-level cloudiness, and the strength of the mid- and upper-level winds (TE; E02).

First, although as early as the day-2 convective outlook (0728 UTC 2 May) forecasters had been expecting development along the dryline, the moisture gradient and convergence along the dryline did not become particularly intense on the afternoon of 3 May (Table 1) and were even found in multiple bands (Figs. 1b–d; TE). When lasting convection occurred, it developed tens of kilometers to the east of the moisture gradients (Fig. 1c). The expected intensification of the dryline did not occur, so what role, if any, did the dryline play in convective initiation?

Second, the cirrus shield that was approaching western Texas and Oklahoma (Fig. 1a) was forecast to limit

surface heating (Table 1). Indeed, the first deep convection developed in north Texas within gaps in the cirrus shield. Although this convection soon dissipated (Fig. 1c), the next convection that developed within this gap (near Lawton, Oklahoma) would become supercell storm A (Figs. 1c,d). What role did the cirrus shield play in the evolution of the outbreak?

The final factor was the strength of the mid- and upper-level winds (Table 2; TE; E02). Because the short-wave trough/jet streak traveled over the relatively data-sparse Pacific Ocean, northern Mexico, and desert Southwest, initialization errors in the operational models concerned the forecasters. Although the upper-level winds were strengthening over Oklahoma through the day on 3 May, their eventual maximum strength was unclear. Around 1246 UTC 3 May, forecasters first had an indication that the winds would be stronger than was projected by previous runs of the National Centers for Environmental Prediction (NCEP) operational forecast models when the SPC day-1 convective outlook stated, ''middle–upper-level winds across southwestern CONUS [continental United States] on both sides of this [short-wave trough] were significantly underforecast by 00Z/03Z Eta, based on latest raob [rawinsonde] data and observations from regional VWP [velocity–azimuth display (VAD) wind profiles from Weather Surveillance Radar-1988 Doppler (WSR-88D)]/ACARS [Aircraft Communications and Reporting System]. AVN [NCEP Aviation run of the Global Spectral Model] winds/heights are verifying much better this morning and suggest mid/upper level flow may be stronger than forecast by Eta over southern Plains this evening.'' Further proof that the winds would be stronger than forecast was evident from the wind profiler network later in the afternoon (section 2b in TE). By 0000 UTC 4 May, these winds were 10–15 m $s^{-1}$ greater than forecast (Figs. 10 and 11 in TE; Fig. 6 in E02).

These winds could play three roles in the resulting convection. First, the incoming jet streak provides a forcing mechanism for upper-level synoptic-scale ascent and the development of cirrus, reducing insolation and slowing the removal of the low-level capping inversion. Second, the low-level synoptic-scale ascent associated with the jet streak favors the removal of the cap through adiabatic cooling, which would counter the cloud-radiative effects and *promote* the development of deep, moist convection. Third, the strength of the incoming winds affects the magnitude of the deep-layer shear and storm organization. The presence of winds stronger than anticipated gave the forecasters confidence that, if storms were to erupt, they would be supercellular and possibly tornadic (Table 2; E02).

In this paper, observations are compared with forecasts from a high-resolution (2-km horizontal grid spacing) numerical weather prediction (NWP) modeling system to understand better the role of the three synoptic processes (dryline, cirrus shield, and the approaching short-wave trough/jet streak) in the 3 May outbreak. This modeling system will be operated in a forecasting mode using initial conditions and lateral boundary conditions derived from forecast data (see section 2 for details). The goal is to understand how these three processes affected the initiation and mode of convection for the event, using tools that might be available to forecasters in the future.

The format of this paper is as follows. In section 2, details concerning the characteristics of the storm-scale numerical model are presented. Section 3 presents the results from the ''control'' forecast and its relationship to the available observations. In section 4, the sensitivities of this forecast to uncertainty in the strength of the short-wave trough/jet streak and the effects of the cirrus shield are explored. The implications of these results for the use of high-resolution models in operational forecasting environments are discussed in section 5. Section 6 is a concluding summary.

## 2. Methodology

Anthes (1986) hypothesized that, in at least some regions and at some times, the mesoscale may be dominated by synoptic-scale processes and may therefore be relatively predictable [see Gall and Shapiro (2000) for further discussion of this point]. There is now evidence to support this hypothesis for certain kinds of events at lead times beyond the nowcast range (e.g., Bélair et al. 1994; Ziegler et al. 1997; Ballentine et al. 1998; Colle et al. 1999; Gallus and Segal 1999; Roebber and Gehring 2000; Colle and Mass 2000; Roebber and Eise 2001; Fowle 2001).

It is understood, however, that initial-condition uncertainty imposes a serious constraint on synoptic-scale predictability for short-range forecasts. Any analysis will not represent the *true* initial state, and, with poor observational coverage in the area upstream of the region of interest, as in the case of 3 May, analysis errors are likely to be substantial. Given generally accepted rates of error growth (e.g., Doswell 1986a; Wandishin et al. 2001), an $O$(24 h) model forecast at scales sufficient to resolve supercell convection will likely be very sensitive to those unresolved details. These forecasts may be most useful in developing a conceptual model of the situation rather than providing explicit predictions of individual storms (Brooks et al. 1992). The emergence of meso- and storm-scale details in the wind, cloud, and precipitation fields of such forecasts may indicate real features in the atmosphere, although not necessarily in the right place nor at the right time. Such a forecast might then be used to understand processes critical to the development of the event under consideration.

An example is provided by Roebber and Eise (2001), who studied a 100-yr flooding event in southeastern Wisconsin, using 24-h simulations. Although it was not possible to predict explicitly individual convective elements at those timescales, the aggregate effects of

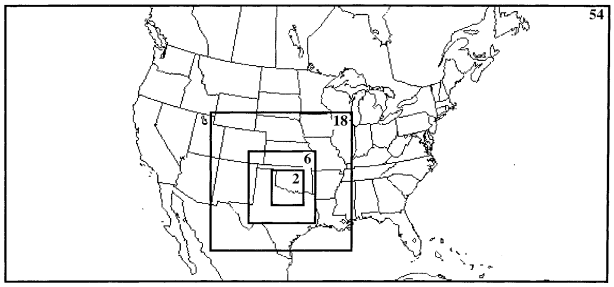


FIG. 2. Quadruply nested domain configuration used in the MM5 forecasts. The horizontal grid spacing (km) is denoted in the upper-right corner of each of the four domains.

training convection were simulated well in a high-resolution (1.67-km horizontal grid spacing) domain. At coarser resolution (5-km grid spacing), although precipitation amounts were substantially underrepresented, the focus of the observed precipitation along an axis of moisture convergence was captured.

Use of models in this way represents a conceptual departure from the goal of deterministic prediction that, by definition, seeks the explicit prediction of sensible weather. In the case of storm-scale models, explicit prediction would include the location and timing of convective initiation for specific storms, the subsequent mode of these storms, and resultant sensible weather (such as peak winds and the spatiotemporal distribution of precipitation). In this study, the primary concern is not with explicit prediction but rather with the environment in which the convection develops, its nature, and what these properties can reveal about the predictability of the actual event. As will be shown, exploration of these issues in this paper will yield considerable insight into the key forecast problems of convective initiation and mode for the 3 May outbreak.

The model forecasts for this event were generated using a system based on the procedure described by Roebber and Gehring (2000). The Pennsylvania State University–National Center for Atmospheric Research Fifth-Generation Mesoscale Model (MM5) is a nonhydrostatic, primitive equation model (Dudhia 1993; Grell et al. 1994). MM5 was run for 30 h from a cold start with initial and lateral boundary conditions provided by the 0000 UTC 3 May 1999 forecast cycle of the AVN run (Petersen and Stackpole 1989). A key point is that no data in addition to the AVN output (at T126, or ~105-km horizontal resolution) were used to initialize the MM5 on any of the domains. The MM5 forecasts were conducted in quadruply nested, two-way interactive mode (Fig. 2), such that conditions in an inner domain feed back to the coarse domain, and vice versa, with matching at the nest boundary (Zhang et al. 1986). The outermost domain (D1), with 54-km horizontal grid spacing, was designed to represent synoptic-scale features, with nesting through domain 2 (D2, 18 km) and domain 3 (D3, 6 km), down to domain 4 (D4) with 2-km horizontal grid spacing, to resolve the details of individual storm structures. An explicit moisture scheme with prognostic equations for cloud water, ice, rainwater, and snow (Reisner et al. 1998) was employed in all domains for grid-resolvable precipitation. The Kain–Fritsch cumulus parameterization scheme (Kain and Fritsch 1993) was used in the two outermost domains (D1, D2). Radiative processes were handled using a cloud-radiation scheme, in which diurnally varying shortwave and longwave radiative fluxes interact with explicit cloud and clear air, and the surface fluxes were used in the ground energy-budget calculations (Dudhia 1989). The planetary boundary layer was modeled using the high-resolution Blackadar scheme (Blackadar 1979; Zhang and Anthes 1982) coupled with a five-layer soil model (Dudhia 1996). The model had 23 vertical sigma levels, with a relative concentration at the lowest levels to resolve planetary boundary layer structures important to convective initiation. Because the horizontal grid spacing of the model simulations in the present study (2 km) is about two orders of magnitude too coarse to simulate tornadogenesis, whether the modeled storms are capable of producing tornadoes is a topic that cannot be addressed here. Therefore, this study focuses on the synoptic, meso-, and storm-scale features of the 3 May outbreak.

The initial time for the integration was 0000 UTC 3 May 1999 in D1–D3, whereas D4 was switched on at 1800 UTC 3 May 1999 (18 h into the simulation). This approach was dictated by current computer resource limitations; however, because convective initiation did not occur in either the model or nature within the region encompassed by D4 until several hours after this time, the impact of this approach on the forecasts is not expected to be significant. In an operational environment, in which the timing of events is not known ahead of time, sufficient resources may be required to produce complete forecasts on all model domains in the two-way nesting configuration employed here. As a less costly alternative, intelligent placement in space and time of a focused domain such as D4 could be accomplished 12–24 h prior to a forecast event, based upon anticipated potential for severe weather [as is currently done with Geostationary Operational Environmental Satellite (GOES) rapid-scan coverage]. More discussion of operational issues is provided in section 5. Data were output for analysis every hour in D1–D3 and every 10 min in D4. Additional forecasts were generated using perturbed initial conditions and varying model physics schemes and are detailed in section 4.

## 3. Evaluation of the control model forecast (CNTL)

In this section, the fidelity of the full-physics model run starting from the unmodified AVN initial state (hereinafter CNTL) is explored. The evolution of the dynamic tropopause, the distribution of precipitation, and the initiation and mode of convection are examined.

### *a. Tropopause evolution*

Figure 3 presents the forecast pressure on the dynamic tropopause [1.5 potential vorticity (PV) unit surface], derived from CNTL. For further information about maps of the dynamic tropopause and their interpretation, see Morgan and Nielsen-Gammon (1998). The 0000 UTC 3 May 1999 dynamic-tropopause analysis (Fig. 3a) shows a strong positive PV anomaly (recognizable as higher pressure on the dynamic tropopause; hereinafter the northern anomaly) embedded within the polar flow over the Pacific Northwest/California and a PV filament (associated with a short-wave/jet streak in the southern stream; hereinafter the southern anomaly) offshore of Baja California. By 1200 UTC 3 May (Fig. 3b), the southern anomaly/jet streak was forecast to weaken as it began to merge with the northern anomaly in the large-scale confluent flow over the southwest United States and northern Mexico. By that evening (Figs. 3c,d), the forecast position of the southern anomaly indicated that this feature, through potential vorticity advection and resultant synoptic-scale ascent, was of possible importance to the events of 3 May. As noted in section 1, the forecasters recognized that the southern anomaly/jet streak was a key feature in this forecast.

The verifying tropopause ''analysis'' [derived from the 0–3-h forecasts of the University of Wisconsin—Milwaukee (UWM) real-time modeling system (Roebber and Gehring 2000), with initial and lateral boundary conditions obtained from the 0000 UTC 4 May 1999 forecast cycle of the AVN run] shows that the broad features of the flow are captured in CNTL (cf. Figs. 3d, 4a,b). However, subtle differences in the pressure on the dynamic tropopause result in variations in the implied PV advection between CNTL and the 0–3-h forecasts. Although these differences are small from the perspective of the synoptic scale, the forecast was remarkably sensitive to these details, as will be shown in section 4.

### *b. Precipitation*

The accumulated precipitation for the 9-h period of 1800 UTC 3 May–0300 UTC 4 May 1999 in CNTL is compared with the observations (Figs. 5a,b). (Although some stratiform precipitation can be expected to accompany convective episodes, the precipitation signature in cases such as this provides a reasonable measure of overall convective activity.) Some supercells persisted beyond 0300 UTC (Fig. 1a of TE), but this period is selected as representative of the initiation and maturation phases of the deep convection that affected Oklahoma. Two swaths of precipitation occurred in north-central Texas in CNTL, consistent with, albeit somewhat to the east of, observations. The bulk of the observed precipitation in central Oklahoma, however, did not occur in CNTL (Figs. 5a,b), representing a serious forecast limitation for explicit prediction of convection. As will be shown in section 4, the location of the storms and accompanying precipitation are sensitive to uncertainties in the analysis of the southern anomaly. However, as will also be shown, considerable information regarding key forecast issues can still be extracted from this imperfect forecast.

### *c. Convective initiation and the role of the cirrus shield*

The evolution of the boundary layer structure leading up to the time of convective initiation in CNTL is similar to nature in three significant ways. First, a double-dryline structure, marked by a somewhat diffuse gradient in dewpoint temperature, existed in northern Texas and Oklahoma (cf. Figs. 1c, 6). Second, convection began within the relatively homogeneous warm, moist air to the east of the dryline boundary (cf. Figs. 1c, 6, 8, 9). Third, low-top cumulus clouds in eastern Oklahoma and Texas were present (cf. Figs. 1a–c, 6). This fidelity with nature suggests that some aspects of convective initiation may be addressable using the model output.

As noted in section 1, a cirrus shield was moving across the region (Fig. 1), and forecasters believed that this cloud might play an important role in the forecast by limiting surface heating. To understand the origin of the cirrus shield, upper-level vertical motion in CNTL is examined. As shown by Barnes et al. (1996), however, applying diagnostics (e.g., PV) to mesoscale meteorological model data results in small-scale features that are unverifiable or model noise. As a consequence, to examine such diagnostics, filtering must be performed. A Gaussian filter, the same as that described in Schultz and Doswell (2000, section 4a), is used, except with an $e$-folding distance of 170 km (a value appropriate for the scale of the PV features to diagnose).

As the southern anomaly moved over Oklahoma, it merged with the northern anomaly and weakened (Figs. 7a–c). By 0000 UTC 4 May 1999, the southern anomaly, in western Oklahoma, was almost completely absorbed into the northern anomaly (Fig. 7d). Nevertheless, the weakening southern anomaly was associated with cyclonic geostrophic PV advection and upward motion (Fig. 7). The leading edge of the cyclonic geostrophic PV advection was nearly coincident with the leading edge of the cirrus shield, with widespread clearing ahead in the region of anticyclonic geostrophic PV advection and descent (Fig. 7). Thus, the model diagnostics indicate that the cirrus shield was due to upper-level forcing for ascent from the deforming PV anomalies.

The relationship between convective initiation and structures in the cirrus shield in the model shows qualitative agreement with observations. A strong cell in the southern part of the domain appears to have formed within a large gap in the cirrus shield (labeled gap A in Fig. 7b; Fig. 8a). This large gap also appears in the observations (Fig. 1a) and may represent a minimum in the upper-level vertical motion in this area (Fig. 7). Twenty minutes later (Fig. 8b), another convective cell

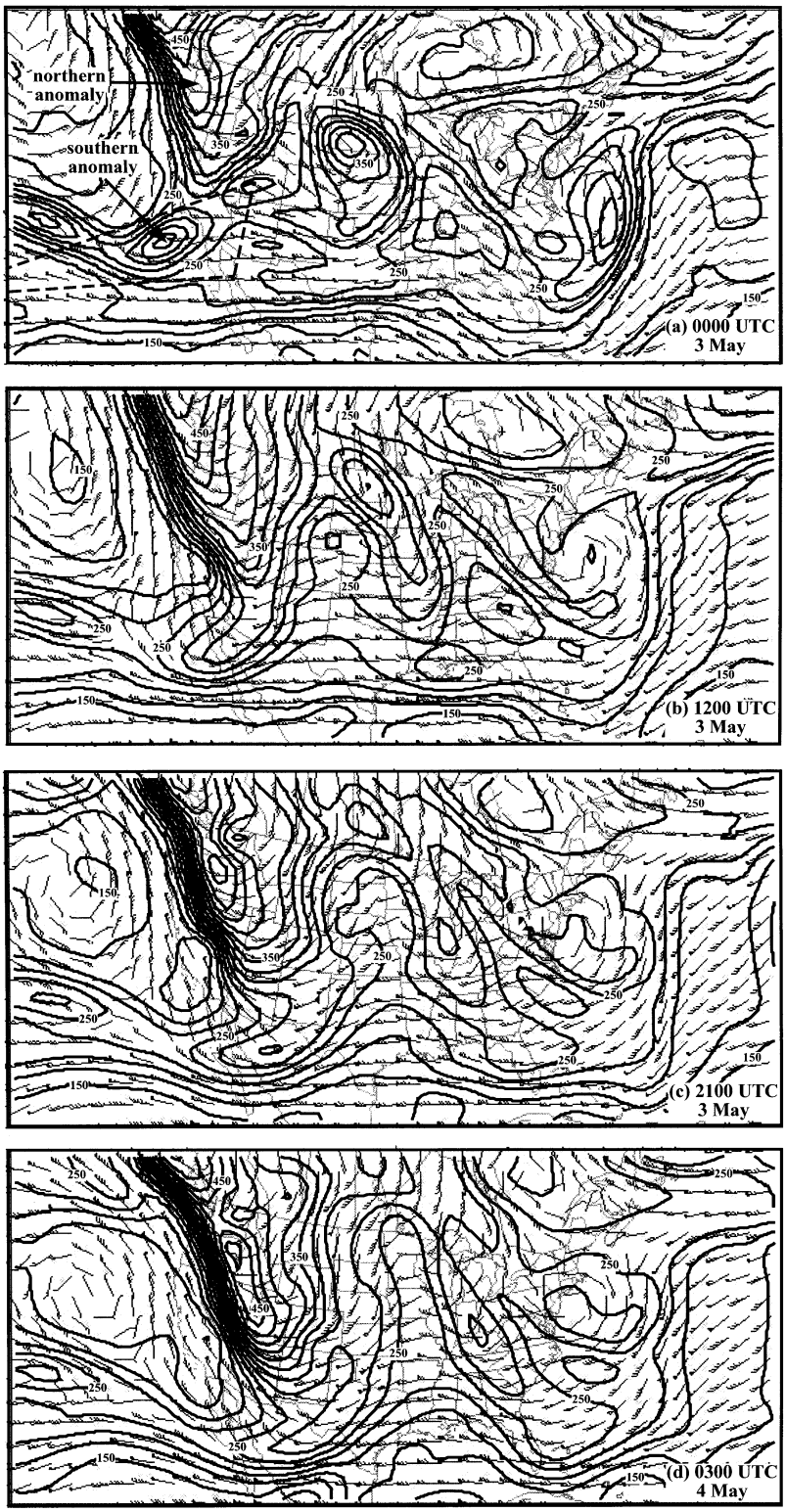


FIG. 3. Pressure (contour interval is 25 hPa) and wind on the dynamic tropopause derived from control forecast (CNTL). The dynamic tropopause is defined as the 1.5-PV unit surface, where 1 PV unit = $1 \times 10^6$ m$^2$ K s$^{-1}$ kg$^{-1}$. Wind barbs are plotted according to the standard meteorological convention (pennant, 25 m s$^{-1}$; long barb, 5 m s$^{-1}$; short barb, 2.5 m s$^{-1}$): (a) 0000 UTC 3 May 1999. The dashed triangle over the Pacific Ocean encloses the area selected as the southern anomaly in the PV-inversion scheme described in section 4: (b) 1200 UTC 3 May, (c) 2100 UTC 3 May, and (d) 0300 UTC 4 May 1999.

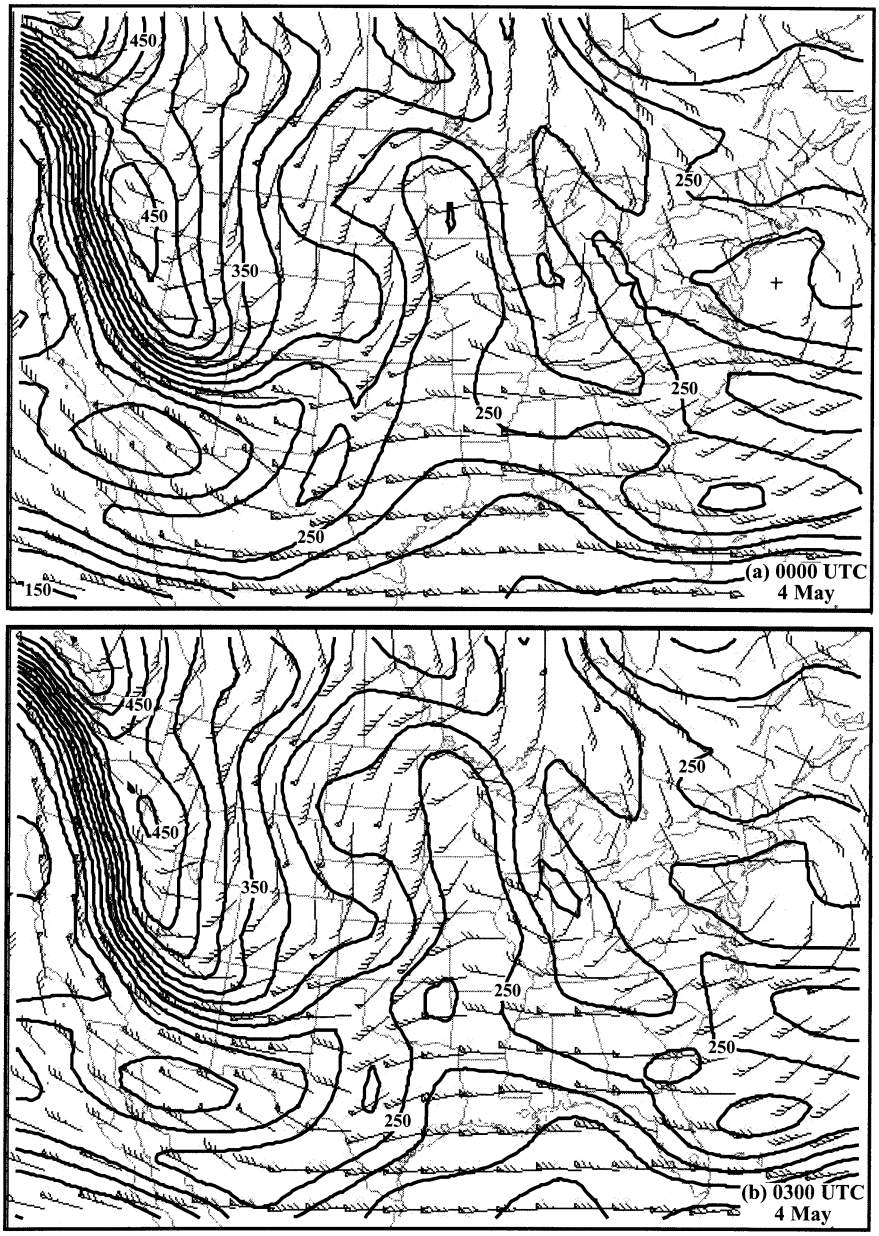


FIG. 4. Pressure (contour interval is 25 hPa) and wind on the dynamic tropopause derived from the 0000 UTC 4 May 1999 run of the UWM real-time MM5 (Roebber and Gehring 2000). The dynamic tropopause is defined as the 1.5-PV unit surface. Wind barbs are plotted as in Fig. 3. (a) The 0-h forecast valid at 0000 UTC 4 May 1999, (b) 3-h forecast valid at 0300 UTC 4 May 1999.

initiates in a smaller gap in the cirrus (labeled gap B in Fig. 7b), just south of the Texas–Oklahoma border and east of the dryline position. This convection persists over the next 40 min, spawning new cells to the southwest (Figs. 8c,d). By 2310 UTC, convective initiation, becoming more widespread, appears to be preferred within the holes (Fig. 8d) of the cirrus shield.

Comparison between the observations (Fig. 1) and CNTL (Figs. 7, 8) shows that in both cases the holes in the cirrus shield occur on two different scales. To be specific, in CNTL, there is a mesoscale gap in the cirrus shield between south-central Texas and just south of the Texas–Oklahoma border (gap A; e.g., Fig. 7b). Gap A is associated with the southern region of convection in CNTL west of Dallas (Figs. 5, 8) and occurs in an area of weaker vertical motion along the southern flank of the broad region of ascent associated with the cirrus production (Fig. 7). In contrast, there are smaller gaps in the cirrus shield on the county scale, for example, gap B (e.g., Fig. 7b). Gap B is associated with the north-

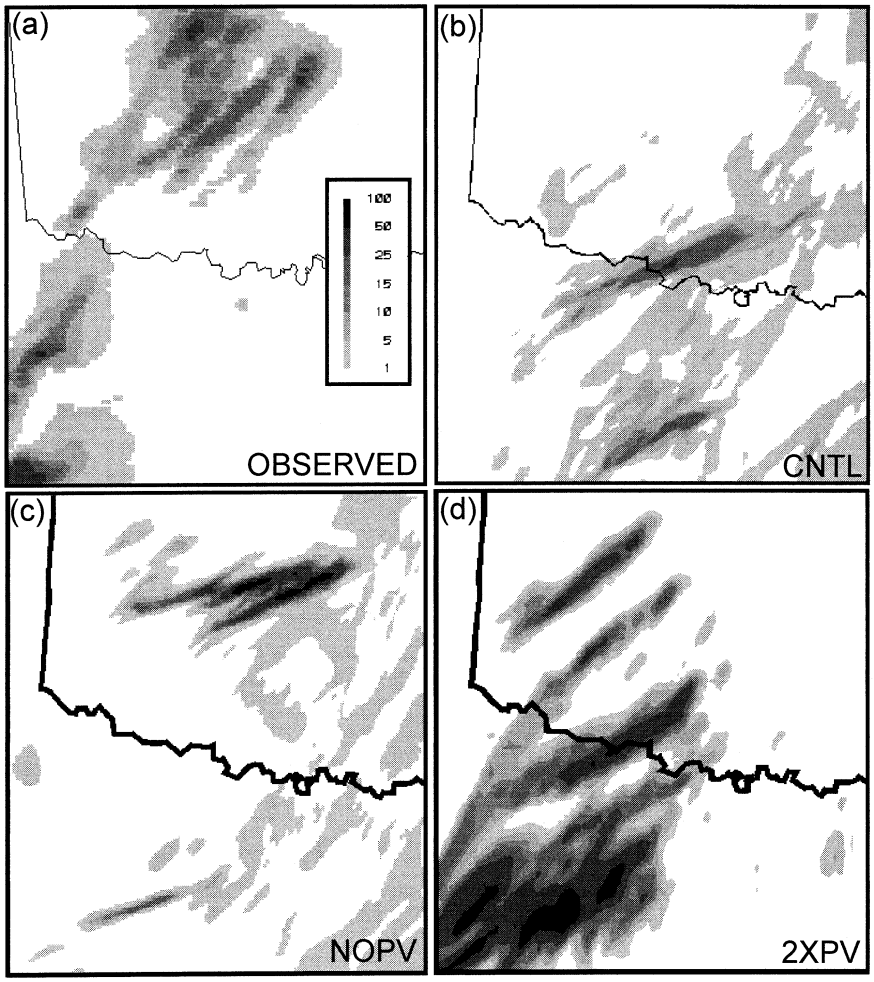


FIG. 5. Accumulated precipitation from 1800 UTC 3 May 1999 to 0300 UTC 4 May 1999 (mm, shaded according to scale in left panel). (a) Observed precipitation, a combination of hourly precipitation–gauge data and radar-derived precipitation [the so-called stage-IV analysis; Baldwin and Mitchell (1997); Fulton et al. (1998)]. (b) Precipitation from the control forecast (CNTL), 2-km grid-spacing domain (D4). (c) Precipitation from the forecast with the southern anomaly removed (NOPV), 2-km grid-spacing domain (D4). (d) Precipitation from the forecast with the doubled southern anomaly (2XPV), 2-km grid-spacing domain (D4).

ern region of convection along the Texas–Oklahoma border (Figs. 5 and 8). The origin of these small-scale gaps, however, is not clear.

To discuss and to quantify these ideas concerning convective initiation, consider the ingredients-based methodology for deep, moist convection proposed by Doswell et al. (1996). These ingredients were identified based upon simple parcel theory: instability, sufficient moisture (to define a level of free convection, LFC), and lift (to bring a parcel to its LFC). Initiation of deep convection is considered to have occurred in D4 at those points at which a local maximum in vertical motion exceeding 1.5 m $s^{-1}$ exists that persists for subsequent time steps (after taking into account storm motion) and is associated with a subjectively determined anvil-like signature in the vertically averaged cloud-ice field. Any events occurring along the outflows of convection were not included in this tabulation. For the period of 1800 UTC 3 May–0000 UTC 4 May, this procedure results in the identification of 11 occurrences of deep convective initiation in D4 (Fig. 9). As suggested by the time-varying model-predicted dryline position (Figs. 6, 8), there is little movement of this feature during this time. None of the 11 convective initiations developed in close proximity to the dryline position (defined by a cell that develops within the ascending branch of the boundary layer vertical motion field collocated with the dryline position at that time), including the ''cloudy'' initiation at 2250 UTC in north Texas (Fig. 9).

The mean convective available potential energy [CAPE; calculated using a virtual temperature correction, following Doswell and Rasmussen (1994) and

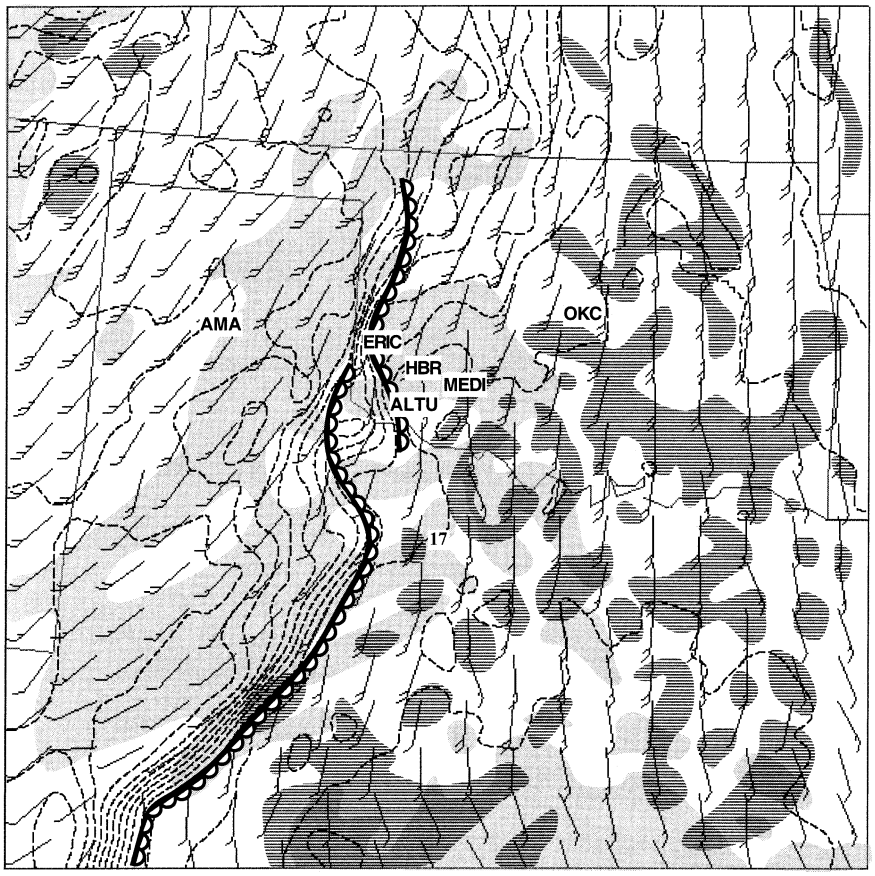


FIG. 6. CNTL 6-km grid-spacing domain (D3), valid at 2100 UTC 3 May 1999, showing vertically averaged cloud-water mixing ratio greater than 0.1 g kg$^{-1}$ (hatched), vertically averaged cloud-ice mixing ratio greater than 0.1 g kg$^{-1}$ (shaded), lowest sigma-level isodrosotherms (dashed lines every 2°C; 17°C contour labeled), and lowest sigma-level winds (as in Fig. 3). The dryline position is defined by the leading edge of the dewpoint temperature gradient greater than or equal to 15°C (100 km)$^{-1}$. The locations of AMA, HBR, OKC, and the Oklahoma Mesonet sites at MEDI, ALTU, and ERIC are plotted.

based on the most unstable parcels in the lowest 300 hPa] at these 11 locations, 10 min prior to model convective initiation, is 3320 J kg$^{-1}$. The mean LFC for these same soundings is 765 hPa, with a lifting depth of 148 hPa. This relatively deep lift requirement results from the presence of a capping inversion, measured by mean convective inhibition (CIN) of 26 J kg$^{-1}$ in the sounding set. Thus, the environment was characterized by considerable buoyant energy with some capping.

It is important to note that the strength of the cap had been decreasing during the time leading up to convective initiation. An example of this evolution is shown in Fig. 10 for two of the locations depicted in Fig. 9. For the sounding in Fig. 10a (Fig. 10b), CAPE increases from 2778 to 3636 (2707 to 3910) J kg$^{-1}$ while CIN decreases from 18 to 8 (12 to 3) J kg$^{-1}$ over the period of 1800–2240 UTC (1800–2320 UTC). The CAPE values are consistent with those in Feltz and Mecikalski (2002), although the CIN values are too small (about 200–300 J kg$^{-1}$ at 1800 UTC). Inspection of the model soundings reveals that the increase in CAPE and weakening of the cap was accomplished through heating at the surface and cooling aloft. The midlevel cooling, which occurred in conjunction with increases in moisture at the same levels, is consistent with the effects of synoptic-scale ascent. Doswell (1987) has suggested that the observed connection between synoptic-scale weather systems and deep moist convection occurs through the moistening and destabilization created by slow but persistent synoptic-scale ascent. At this time, the southern anomaly/jet streak produced ascent on the regional scale (Fig. 3c, Fig. 7). Neglecting horizontal advections, the ascent implied by the cooling over the 800–500-hPa layer from 1800 to 2250 UTC in the sounding of Fig. 10a is 2.9 cm s$^{-1}$. The corresponding ascent for the 750–450-hPa layer from 1800 to 2330 UTC in Fig. 10b is 2.2 cm s$^{-1}$. Given the lifting depths noted above, this ascent is too slow to initiate convection (~12 h); clearly, its primary effect is to work in com-

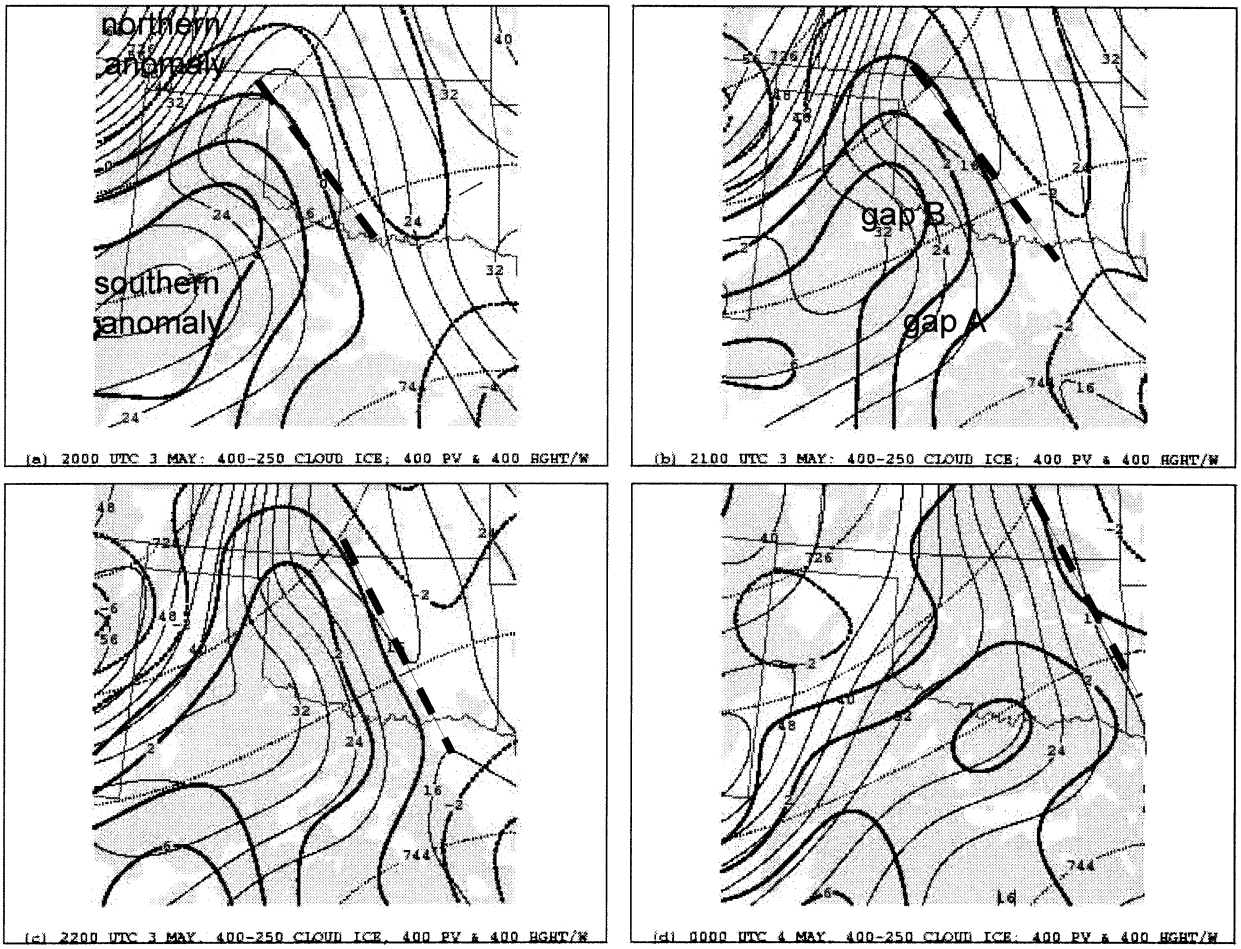


FIG. 7. CNTL 6-km grid-spacing domain (D3): 400–250-hPa layer average cloud-ice mixing ratio (shaded greater than 0.1 g kg$^{-1}$), 400-hPa filtered height (dotted lines, every 6 dam), 400-hPa filtered potential vorticity (thin solid lines, every $4 \times 10^{-8}$ m$^2$ K s$^{-1}$ kg$^{-1}$, or 0.04 PV units), 400-hPa filtered vertical velocity (thick solid lines, every 2 cm s$^{-1}$), and leading edge of cirrus shield at 300 hPa (thick dashed line). For details of filtering methodology, see text. Northern anomaly and PV filament labeled in (a); gaps in cirrus (A and B) labeled in (b): (a) 2000 UTC 3 May, (b) 2100 UTC 3 May, (c) 2200 UTC 3 May, and (d) 0000 UTC 4 May 1999.

bination with boundary layer warming to weaken the cap further and increase the likelihood of convective initiation given mesoscale lift.

In CNTL, 7 of the 11 convective initiation events occurred to the east of or within a break in the cirrus cloud (Fig. 9). Although in some of these seven instances, individual cirrus breaks are not resident above a particular location for extended periods, these locations experienced repeated exposures to such breaks. This aspect is documented by measuring the percentage of maximum insolation for the period from 1800 UTC to the time of convective initiation at these seven locations (69%), as compared with nearby sites in which cirrus existed (58%) or in which both low and high cloud were present (38%). An examination of observed convective initiation for this same area and time period (using radar and satellite imagery), conducted by one of the authors (DMS) without knowledge of the model results, also revealed 11 cases of convective initiation, of which 7 occurred in cirrus breaks. Data from the Oklahoma Mesonet reveal high percentages of maximum insolation near the initiation locations of storm A and storm B [68% and 75%, at Medicine Park (MEDI) and Altus (ALTU), respectively], and a much lower value where convection did not occur [e.g., 46% at Erick (ERIC), a station to the northwest of ALTU; see Fig. 6].

The two soundings at model convective initiation sites (Fig. 10) experienced warming in the boundary layer, with the greatest warming occurring at the relatively cloud-free location (Fig. 10a). This location experienced 70% of the maximum possible insolation from 1800 UTC to the time of convective initiation (2250 UTC). In contrast, the location of the sounding in Fig. 10b was cloud covered during much of this time, resulting in only 40% of the maximum possible insolation. As noted above, both locations were within the region in which synoptic-scale ascent was occurring, yielding similar cooling aloft in the two cases. As a result, in-

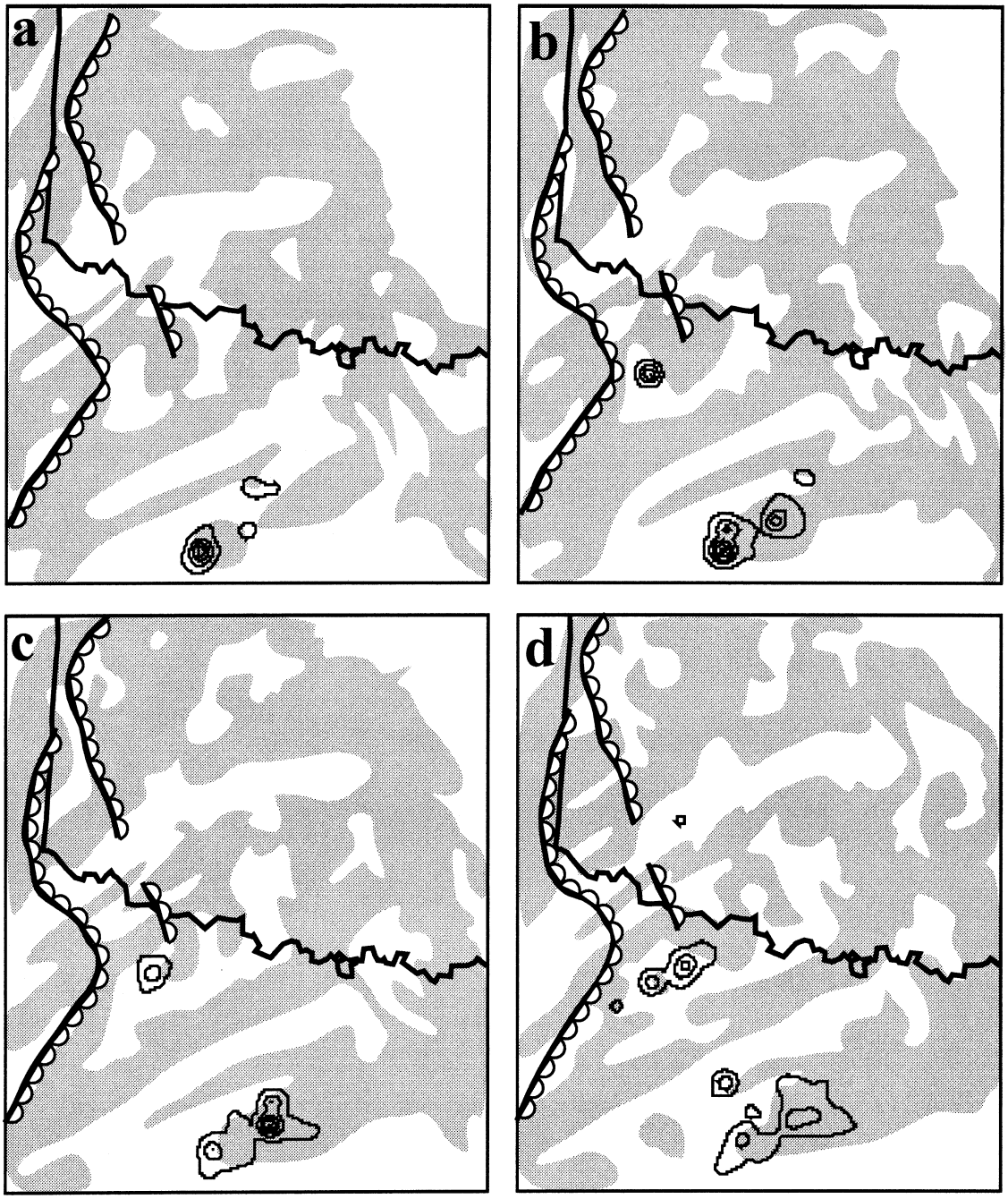


FIG. 8. CNTL 2-km grid-spacing domain (D4) 400–250-hPa layer average cloud-ice mixing ratio greater than 0.1 g kg$^{-1}$ (shaded) and maximum vertical velocity in column (2 m s$^{-1}$ contour interval; first contour at 1 m s$^{-1}$) at (a) 2210, (b) 2230, (c) 2250, and (d) 2310 UTC 3 May. The time-varying model-predicted dryline position is defined by the leading edge of the dewpoint temperature gradient greater than or equal to 15°C (100 km)$^{-1}$.

creases in CAPE and decreases in CIN were comparable at the two sites, leaving both locations more susceptible to convective initiation than earlier in the day. The median *decrease* in CIN from 1800 UTC to the time of convective initiation was 11 J kg$^{-1}$ for the seven relatively cloud-free sites in CNTL, as compared with 7 J kg$^{-1}$ for the four cloudy sites, suggesting the contributory, but nonessential, nature of the cirrus breaks to the process of convective initiation. This is confirmed by noting that four cases in both the model and nature occurred despite the reduction of insolation by the cloud cover, while some areas in which the insolation was not obstructed did not experience convection. Rather, the boundary layer heating appears to have been a contrib-

uting factor in an environment characterized by weak capping, but in which organized mesoscale lift was lacking.

Despite the apparently favorable environment (substantial CAPE, negligible CIN as a consequence of the erosion of the cap), note that the cloud-free storm initiation (labeled a in Fig. 9) persists for only 60 min and does not develop supercellular structure (Figs. 5b, 11). The bulk Richardson number shear (BRNSHR) and storm-relative helicity (SRH) for the time of convective initiation at this location were 257 and 114 $m^2\ s^{-2}$, respectively, values marginally consistent with the development of supercells (Brooks et al. 1994; Stensrud et al. 1997) and similar to profiler observations at Purcell, Oklahoma, from this time (TE). The failure of this storm to persist may result from model deficiencies but alternatively may reflect physical reasons unrelated to model errors. For example, it may be that the shear was too strong to allow a quasi-steady balance between the updraft and the outflow from being achieved in this particular storm (Stensrud et al. 1997). A complete analysis of this question, however, is beyond the scope of this paper.

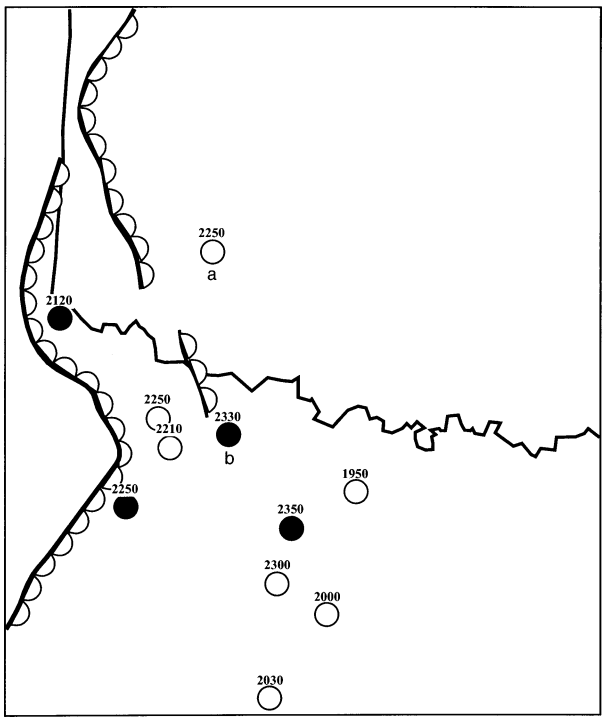


FIG. 9. Sites of convective initiation in CNTL for 1800 UTC 3 May 1999–0000 UTC 4 May 1999. Open (filled) circle denotes cloud-free (cloud covered) site. The time (UTC) of convective initiation is indicated. The dryline position at 2210 UTC is plotted and is defined by the leading edge of the dewpoint temperature gradient greater than or equal to 15°C (100 km)$^{-1}$. Thermodynamic diagrams from the sites denoted a and b are plotted in Figs. 10a,b, respectively.

### *d. Supercellular structure*

Once convection begins in CNTL, many of the storms exhibit vertical-motion and cloud-ice characteristics that are qualitatively similar to that of supercell storms (e.g., cf. Figs. 1d, 8d). Lemon and Doswell (1979) discuss the development of a divided updraft structure in mesocyclones. With 2-km grid spacing, such finescale details are not resolvable except in the largest cells. However, linear and semilinear theories (Davies-Jones 1984; Rotunno and Klemp 1985) predict a positive correlation between vertical velocity and vertical vorticity in an isolated updraft when the low-level environmental vorticity has a significant component in the direction of the storm-relative winds. This correlation has been used as a working definition of supercells in many studies (e.g., Weisman and Klemp 1984; Vasiloff et al. 1986; Droegemeier et al. 1993; McCaul and Weisman 1996; Weisman and Rotunno 2000). Consistent with this work, the following supercell criteria are constructed:

1) the correlation between positive vertical motion (for all points in a 64-$km^2$ area for which the updraft is greater than 1 m $s^{-1}$) and vertical vorticity is computed every 500 m from the surface to 12 km; this correlation must be greater than or equal to 0.5 in each of three or more successive vertical levels;
2) the first criterion must be met for at least six consecutive 10-min intervals; and
3) the first two criteria must be met in association with a major updraft, defined by vertical motion greater than or equal to 5 m $s^{-1}$ at all times during the storm lifetime.

The first criterion is similar to that employed by Droegemeier et al. (1993) and Weisman and Rotunno (2000) in their studies of storm structural characteristics using three-dimensional cloud models with 1-km horizontal grid spacing. The second criterion is applied to prevent the identification of rotating updrafts that do not exhibit substantial temporal persistence, because sustained vertical correlation between vertical vorticity and vertical velocity is a marked characteristic of supercells (e.g., Droegemeier et al. 1993). Although the minimum time period required to satisfy criterion 2 is still less than the typical life spans of observed supercells, in practice (detailed below), most of the identified supercells in the model persisted longer than this minimum period. The third criterion is used to restrict the set to the strongest storms. Although this minimum vertical motion is not strong in comparison with estimated maximum storm updrafts in nature and cloud models of 30–60 m $s^{-1}$ (e.g., Bluestein et al. 1988; Atkins et al. 1999), this criterion applies to all times in the identified storm lifetime. It should be noted that the average maximum vertical motion in the storms identified using these three criteria is 30 m $s^{-1}$, with vertical motions exceeding 44 m $s^{-1}$ in one model storm (an example of the results of this storm tracking is shown in section 4, Fig. 19).

Applying criteria 1–3 to output from D4 in CNTL from 1800 UTC 3 May to 0600 UTC 4 May 1999 results

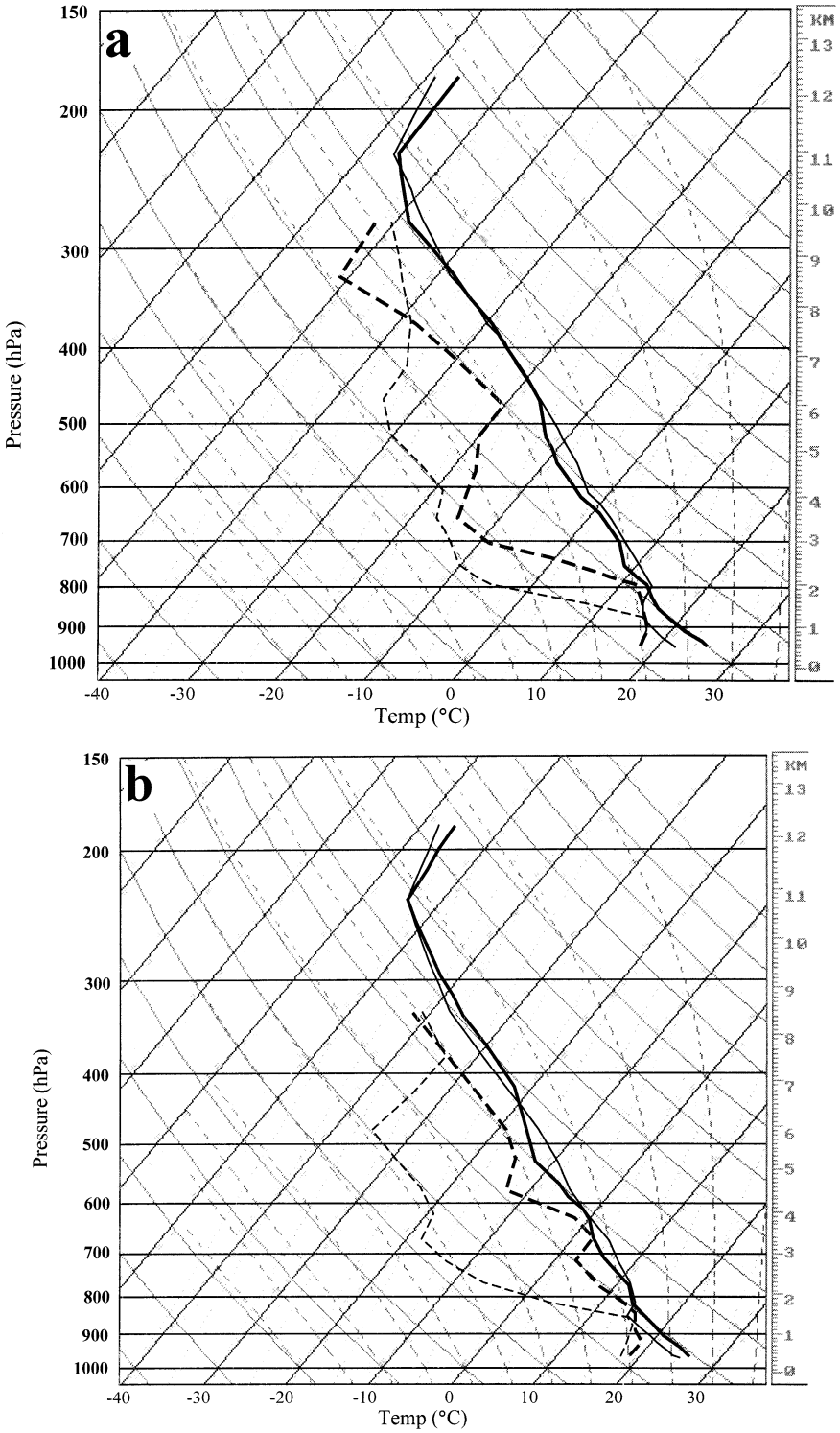


FIG. 10. Thermodynamic diagrams for the sites denoted (a) and (b) in Figure 9. Shown are temperature (solid) and dewpoint temperature (dashed) at 1800 UTC (thin lines) and 10 min prior to the time of convective initiation (thick lines).

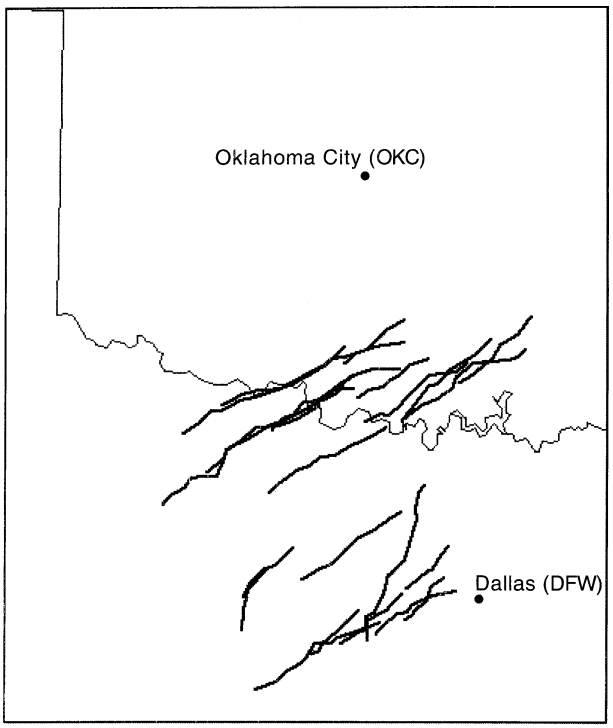


FIG. 11. CNTL supercell tracks (22) diagnosed from 2-km grid-spacing domain (D4) for 1800 UTC 3 May 1999–0600 UTC 4 May 1999 (see text for details).

in the identification of 22 supercell storms (Fig. 11), of which 11 occur near the Texas–Oklahoma border. Thompson and Edwards (2000, their Fig. 1) approximated the lifetimes of the 10 tornadic supercells during the 3 May 1999 outbreak from radar reflectivity of storm initiation and decay, either by dissipation of the cell or by merger of the cell into a larger convective mass with loss of a distinct identity to the cell (R. Edwards 2001, personal communication). The lifetimes for these 10 storms ranged from 120 to 405 min, with a median life span of 203 min. At any given time, as many as seven storms existed. Of these storms, the longest track was ~250 km. By comparison, of the 11 supercells in CNTL near the Texas–Oklahoma border, the lifetimes range from 60 to 170 min, with a median life span of 90 min. In the model forecast, as many as five storms exist simultaneously in this region. Of these model storms, the longest track is 160 km.

To our knowledge, a climatological study of model supercell lifetimes in evolving large-scale environments has never been made, and, as a result, there is no objective measure of what would constitute an exceptional model supercell lifetime. The model supercells, although long lived, clearly did not persist as long as in nature. Nevertheless, a forecaster viewing Fig. 11 and the above statistics would likely conclude that there was a distinct possibility in this case of an outbreak of long-lived, long-track supercells. The inference could then be made that these model storms would be more likely to produce tornadoes, especially strong and violent ones (Wood et al. 1996).

Note that the 11 cells west of Dallas, Texas exhibited only slightly less impressive statistics than the Texas–Oklahoma-border cells in terms of storm lifetime and length of track. Although severe thunderstorms were observed in Texas during this time (Fig. 11 of E02), there were few reports of tornadoes. Further, the forecast positions of these storms are too far to the east. This location error, identified in section 3a with respect to precipitation patterns (cf. Figs. 5a,b), will be examined further in the next section.

## 4. Synoptic regulation: The roles of the southern anomaly

The southern anomaly had three roles in affecting the events of 3 May 1999. First, the deep-layer horizontal wind shear associated with the southern anomaly would favor the production of supercell storms, given convective initiation. Second, the midlevel synoptic-scale ascent resulting from advection of PV was important in weakening the cap through adiabatic cooling (e.g., Fig. 10). This weakening of the cap would tend to promote deep convection. Third, the upper-level ascent resulting from the PV advection produced the cirrus shield (section 3c). Observations and CNTL both showed that convective initiation was slightly more likely to occur in areas with greater insolation, with reductions in CIN in these same areas in CNTL (section 3c). Hence, the production of cirrus would inhibit widespread storm development.

To examine these effects, two sensitivity simulations are performed. The first sensitivity simulation (NOPV) is identical to CNTL, except that the southern anomaly is removed from the initial conditions (0000 UTC 3 May 1999) following the procedure to be described below. NOPV allows a direct examination of the effects of the absence of the southern anomaly on the forecast. The second sensitivity simulation (2XPV) is identical to CNTL, except that the southern anomaly is doubled in magnitude, again as described below. This simulation provides a means of assessing the role of ''weak'' versus ''strong'' synoptic forcing on the evolution of the event, especially as it relates to the initial-condition uncertainty concerning this feature.

### *a. Potential vorticity surgery*

Ertel PV, or simply PV, is a measure of a fluid that incorporates its thermodynamic and hydrodynamic properties. If the fluid is adiabatic and frictionless, then PV is conserved following the flow and so serves as a tracer of the fluid motions. Given an appropriate balance condition (e.g., gradient wind) and boundary conditions, the invertibility principle (e.g., Hoskins et al. 1985) allows the unique recovery of winds and temperatures from a PV field. In this regard, atmospheric structure

can be thought of as a superposition of positive and negative PV anomalies, with the observed wind field being the result of the sum of all the wind fields associated with each PV anomaly separately (Bluestein 1993, 187–195). Hence, a dynamically consistent way to examine the effects of the southern anomaly is to perform ''surgery'' on the PV field through invocation of the invertibility principle. In this regard, our methodology resembles that of Huo et al. (1999a,b), who explored the role of the participating PV anomalies in the 13 March 1993 ''Superstorm.'' The methodology to alter the PV structure of the initial conditions in this study is that described by Romero (2001, section 3). To identify the southern anomaly, the Ertel PV is computed on D1 for every 3 h from 0000 UTC 3 May to 0300 UTC 4 May 1999. Time-mean PV over this 27-h period is defined, and departures from this time mean are examined at 0000 UTC 3 May 1999. The relevant southern anomaly for the outbreak is defined as the area in which the departure is greater than 0.5 PV units (1 PV unit = $10^{-6}$ m$^2$ s$^{-1}$ K kg$^{-1}$) between 150 and 600 hPa and bounded by three line segments enclosing the anomaly as it resides over the Pacific Ocean at 0000 UTC 3 May (Fig. 3a). As cautioned by Lackmann (2002), care is taken to ensure that spurious PV gradients are not created by the removal of the southern anomaly from the total field. After isolating the relevant PV anomaly, piecewise PV inversion is used to calculate the balanced flow associated with the anomaly through the invertibility principle. Using the methodology of Davis and Emanuel (1991), the inversion is performed using the balance assumption of the Charney (1955) nonlinear balance equation. Therefore, to remove the southern anomaly from the initial conditions of the simulation, the balanced fields of the southern anomaly (wind, height, and temperature) are subtracted from the total fields at 0000 UTC 3 May (Fig. 12a). The simulations are then performed with these altered initial conditions (Fig. 12). To perform the 2XPV simulation, the balanced fields associated with the southern PV anomaly isolated in the NOPV run are *added* to the CNTL initial conditions, resulting in a doubling of the initial strength of the southern anomaly (Fig. 13a).

### *b. Direct effects of the southern PV anomaly*

The evolution of the NOPV dynamic tropopause differs in two important ways from CNTL (cf. Figs. 12b,c and 3b,c). First, lacking the southern anomaly, potential vorticity advection across the southwestern United States, north Texas, and southwestern Oklahoma is reduced relative to CNTL. Second, the potential vorticity gradient associated with the northern anomaly extends southeastward more quickly than in CNTL. The resultant precipitation pattern from the NOPV simulation (Fig. 5c) shows a shift in the regional focus of the convective activity northwestward into central Oklahoma. Despite the absence of the southern anomaly and its attendant forcing in NOPV, areas of substantial precipitation occur in that simulation.

The 2XPV simulation accentuates the role of the southern anomaly (cf. Figs. 13c,d, 3c,d, 12c,d). However, in this case, robust advection of potential vorticity across north Texas and Oklahoma results from the strengthened southern anomaly. The 2XPV precipitation distribution is consistent with this advection pattern (cf. Figs. 5d, 13c,d).

To quantify these observations concerning the dynamical environment in which the convection develops in these three simulations (CNTL, NOPV, 2XPV), pressure advection on the dynamic tropopause is computed (Fig. 14). In CNTL, a sequence of increasing pressure (PV) advection from west to east, with peak values of 247 hPa (12 h)$^{-1}$ (Fig. 14a), appears to represent the advections associated with the coalescing northern and southern anomalies (Figs. 3c,d, 7). Although advections in NOPV are weaker [$\sim$100 hPa (12 h)$^{-1}$], these values peak earlier in association with the southeastward extension of the northern anomaly (Fig. 12c). In 2XPV, with the northern anomaly remaining upstream, the advections arise directly from the strengthened southern anomaly, peaking at 369 hPa (12 h)$^{-1}$. The peak advections are delayed somewhat relative to the other simulations, suggesting the delicate nature of the interactions between PV anomalies in confluent flow (e.g., Hakim et al. 1996).

CAPE, BRNSHR, and SRH were calculated for the same three boxes centered on Amarillo, Texas (AMA); Hobart, Oklahoma (HBR); and Oklahoma City (OKC) (Fig. 15). CAPE was defined as that of the most unstable parcel for parcels lifted from the lowest five sigma levels ($\sim$40 m above the surface to $\sim$890 hPa), and SRH was computed in the 0–3-km layer with storm motion defined as 30° to the right and 75% of the 0–6-km mean wind. In CNTL, CAPE increases rapidly during the afternoon hours, reaching peak values of 2917 J kg$^{-1}$ near OKC, with lesser values toward the west resulting from the drier air behind the dryline. BRNSHR rises rapidly during this same time, peaking at 124 m$^2$ s$^{-2}$ at 0100 UTC near HBR. SRH rises from about 100 to 344 m$^2$ s$^{-2}$. It is interesting to note that SRH remained marginal though 2200 UTC and increased substantially only after the time of convective initiation. This evolution in CNTL mirrored the observed conditions and represented a significant diagnostic problem for forecasters on that day (TE).

What is the role of the southern anomaly/upper jet streak in generating deep-layer shear? Contrary to naïve expectation, the effect of the southern anomaly is to *decrease* BRNSHR and SRH (Fig. 15, CNTL vs NOPV). The apparent contradiction of an upper-level jet streak acting to decrease deep-layer shear can be understood through the effects of PV anomaly interactions in confluent flow, as noted above. This result is further accentuated by examination of BRNSHR and SRH for 2XPV. Here, where the jet streak is strongest,

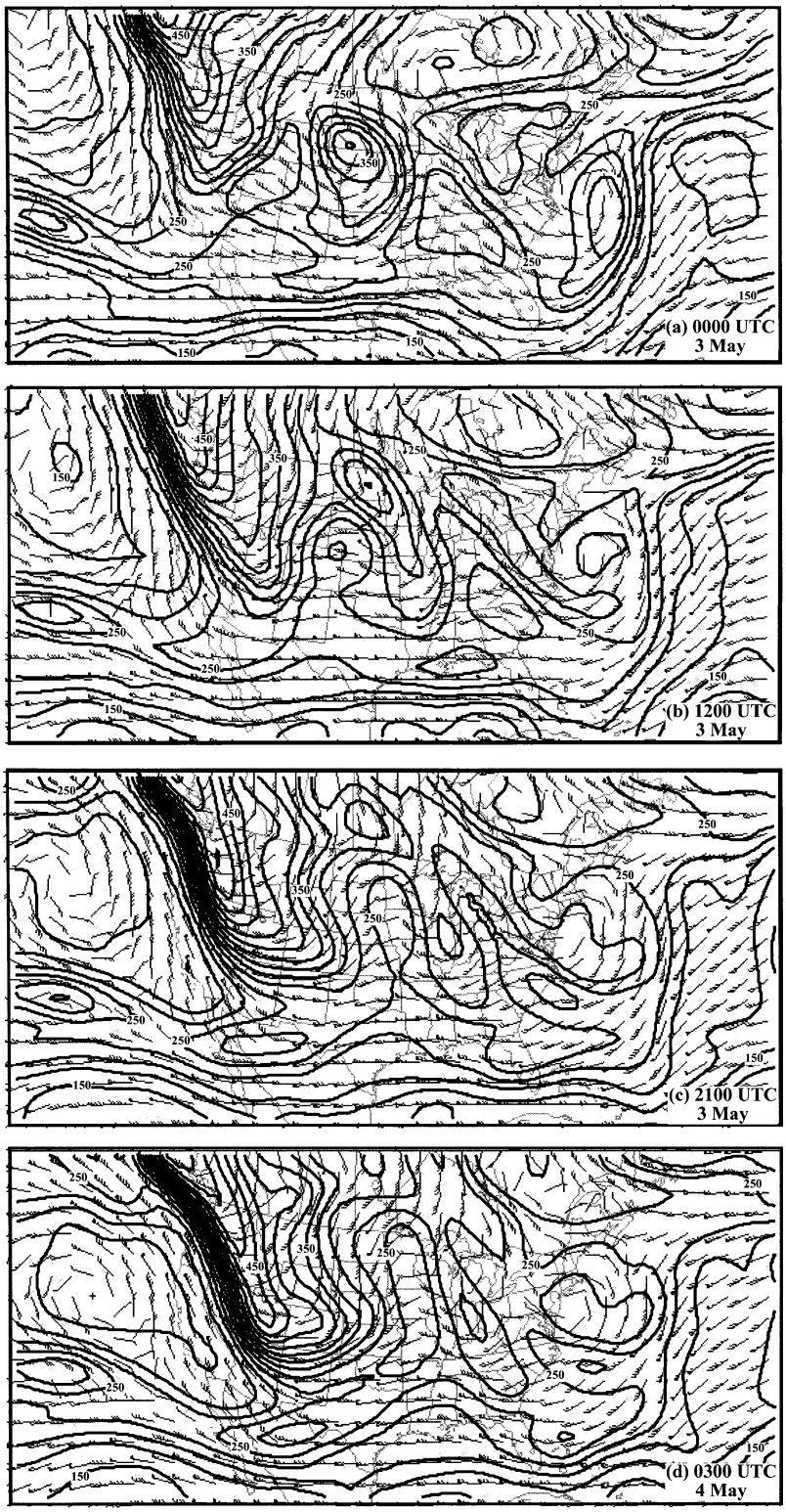


FIG. 12. Same as Fig. 3 but derived from forecast with the southern anomaly removed (NOPV).

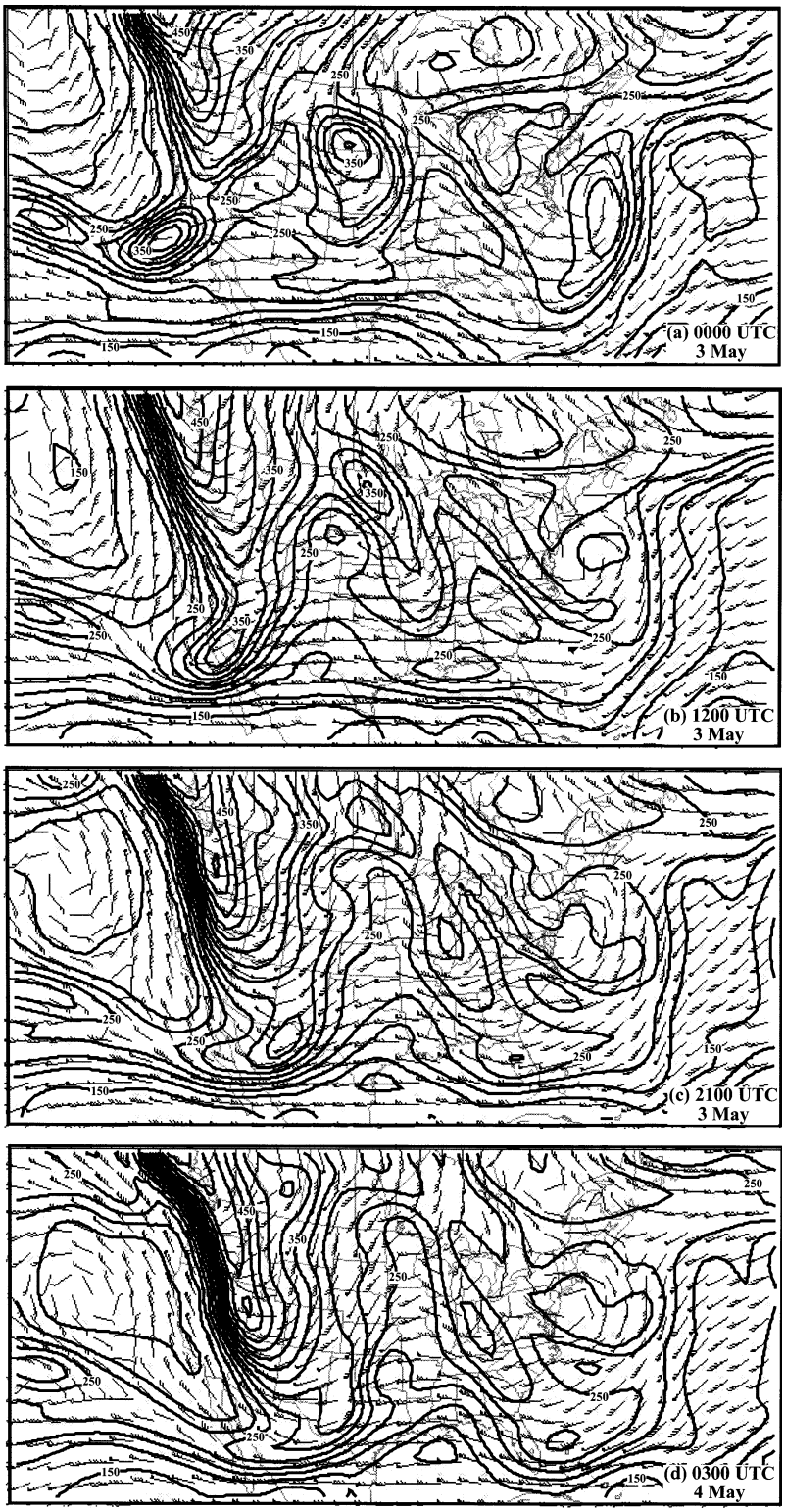


FIG. 13. Same as Fig. 3 but derived from forecast with the doubled southern anomaly (2XPV).

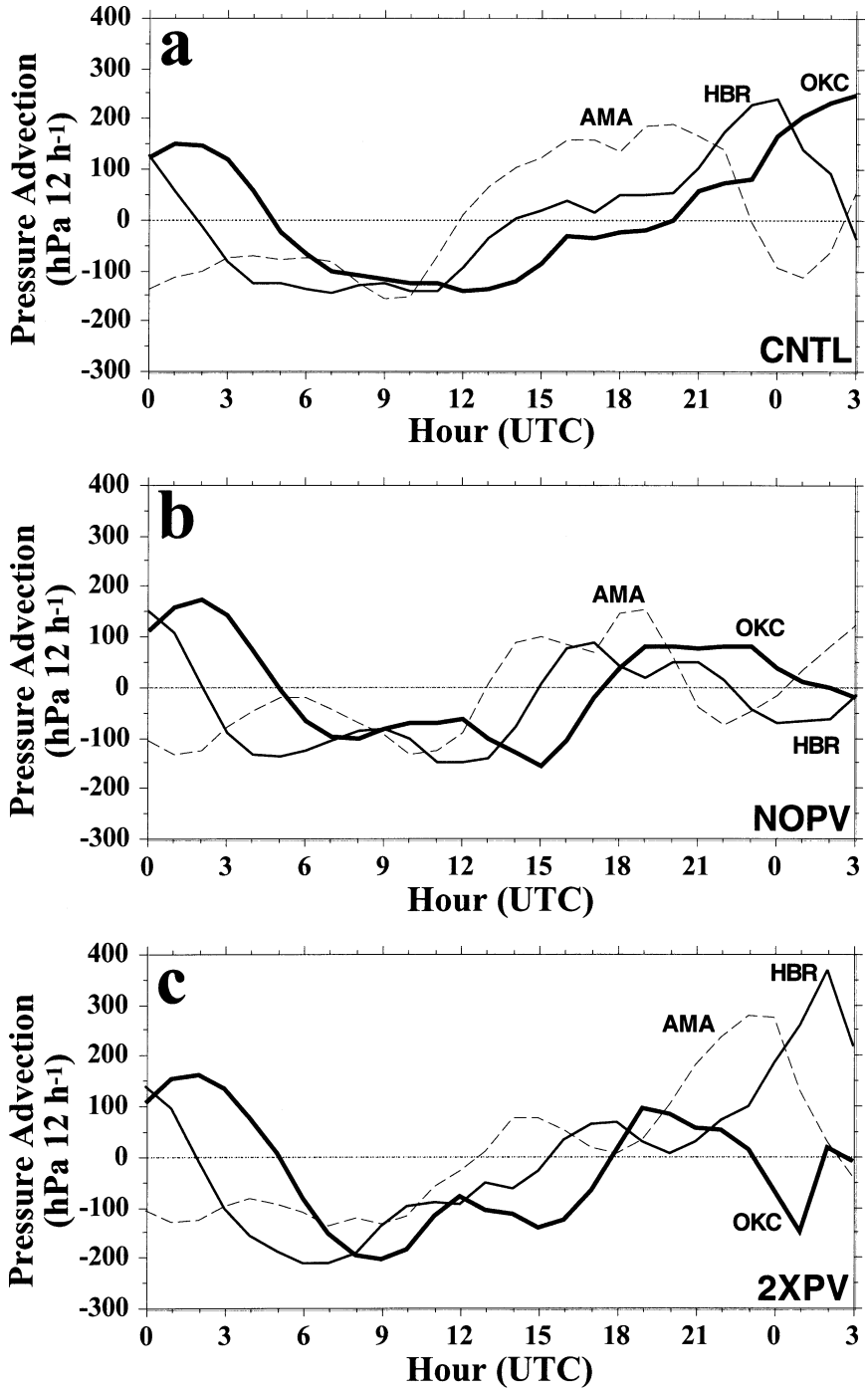


FIG. 14. Time series of pressure advection [hPa (12 h)$^{-1}$] on the dynamic tropopause for 0000 UTC 3 May–0300 UTC 4 May 1999 for (a) CNTL, (b) NOPV, and (c) 2XPV. The dynamic tropopause is defined as the 1.5-PV unit surface. Advections are computed within 216 km by 216 km boxes centered on grid points corresponding to the positions of AMA (dashed), HBR (solid), and OKC (thick solid; see Fig. 6 for site locations).

deep-layer shear is the weakest of the three simulations. The interaction of the strengthened southern anomaly with the strong northern anomaly prevents the latter feature from extending southeastward into the region of interest, keeping shear lower. This issue is of potential importance, since the resulting values of BRNSHR and SRH in 2XPV are only marginally supportive of supercells (Brooks et al. 1994; Stensrud et al. 1997).

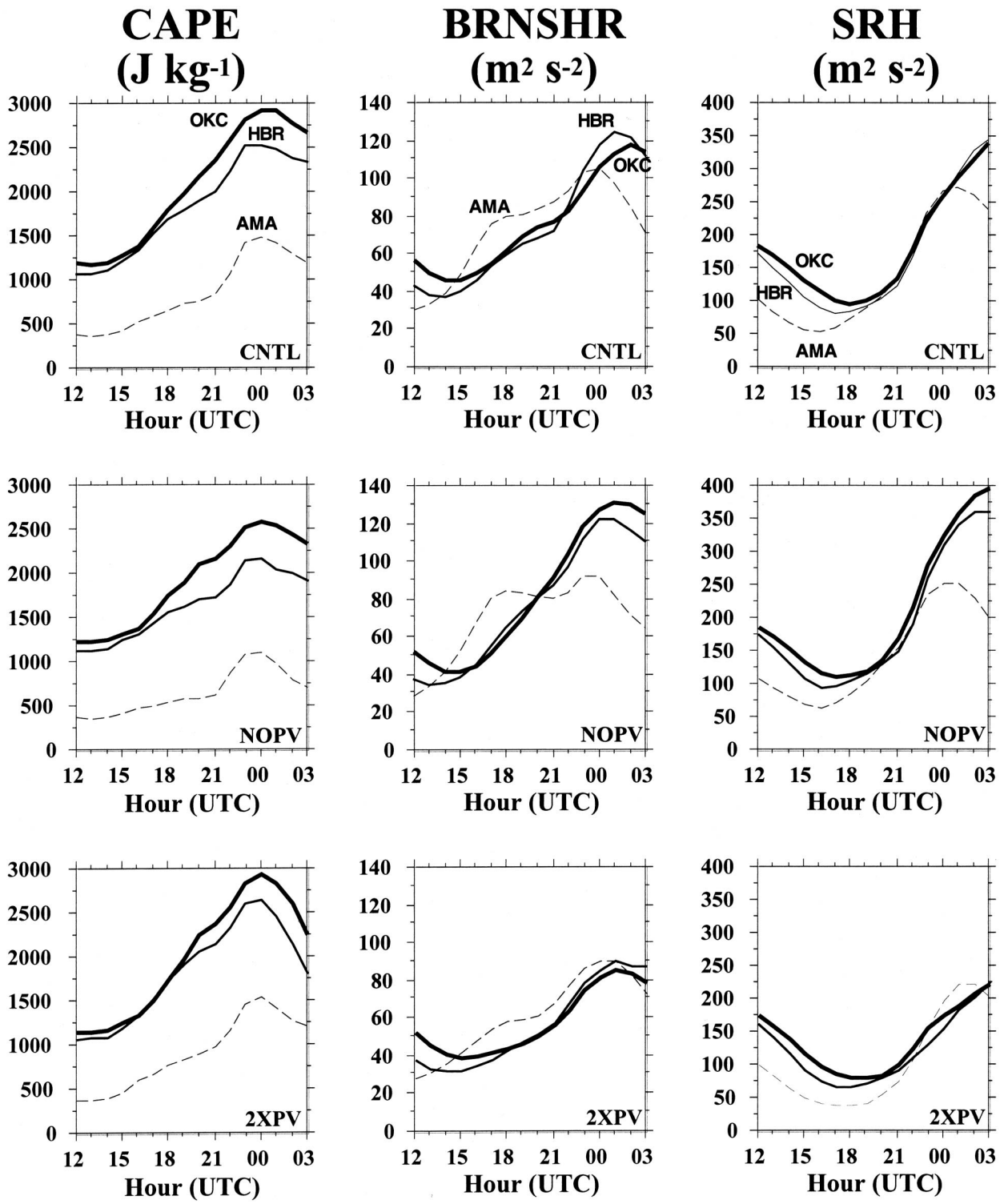


FIG. 15. Time series of CAPE (J kg$^{-1}$), BRNSHR (m$^2$ s$^{-2}$), and SRH (m$^2$ s$^{-2}$) for 1200 UTC 3 May–0300 UTC 4 May 1999 for CNTL, NOPV, and 2XPV. Measures are computed within 216 km by 216 km boxes centered on grid points corresponding to the positions of AMA (dashed), HBR (solid), and OKC (thick solid; see Fig. 6 for site locations).

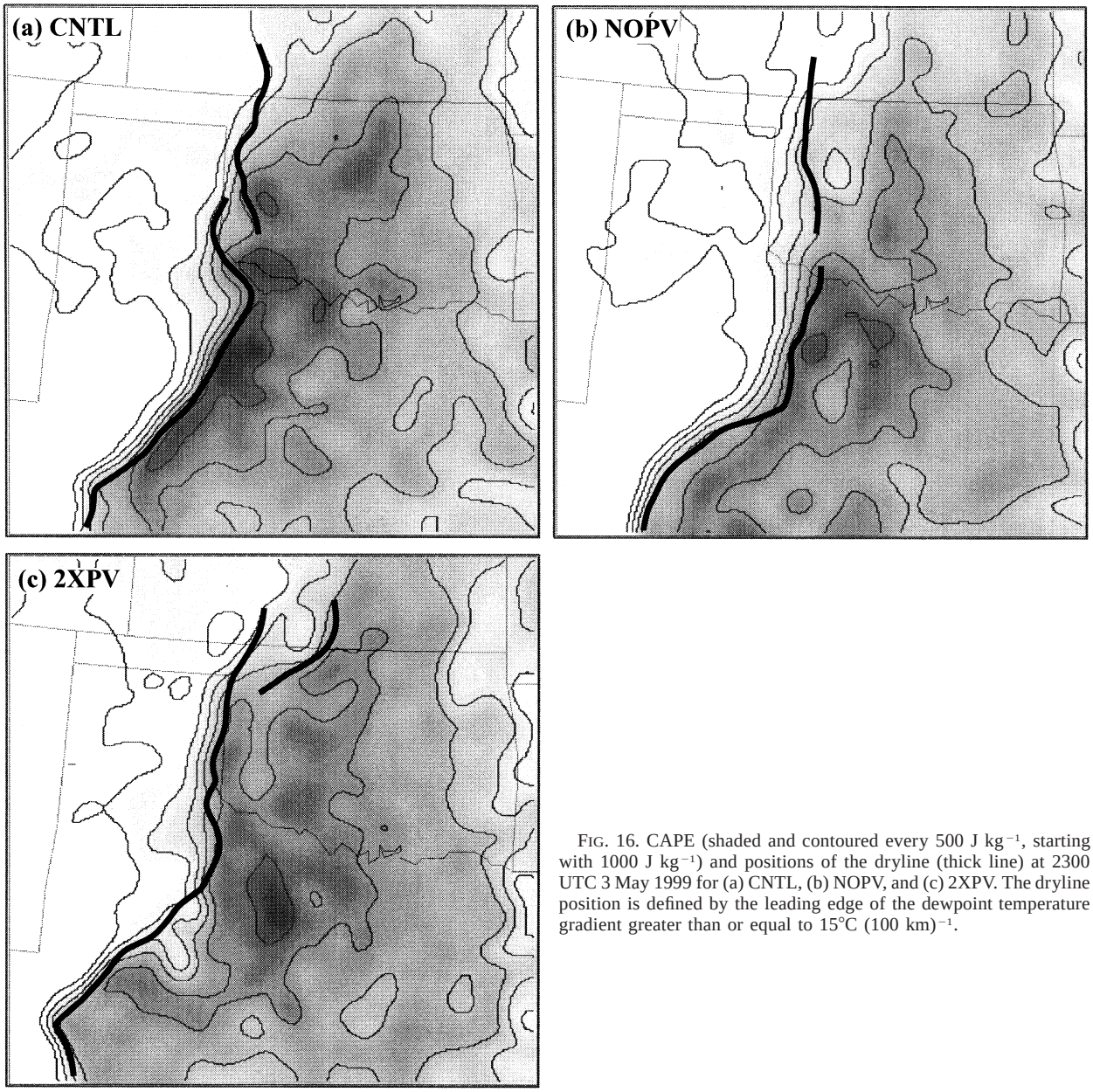


FIG. 16. CAPE (shaded and contoured every 500 J kg$^{-1}$, starting with 1000 J kg$^{-1}$) and positions of the dryline (thick line) at 2300 UTC 3 May 1999 for (a) CNTL, (b) NOPV, and (c) 2XPV. The dryline position is defined by the leading edge of the dewpoint temperature gradient greater than or equal to 15°C (100 km)$^{-1}$.

Thermodynamic conditions are also affected by the southern anomaly. In this case, alterations in average CAPE primarily reflect adjustments in the position of the dryline (Fig. 16). For example, in NOPV, average values of CAPE fall as the dryline shifts eastward, but peak values east of the dryline are unchanged from those in CNTL. In 2XPV, the dryline position remains close to that of CNTL until after 0000 UTC 4 May, and average CAPE values remain similar.

In CNTL, a gradual increase in areal coverage of precipitation occurs through 0300 UTC in southwestern and central Oklahoma, with rain rates peaking at 0200 UTC (Fig. 17). This timing corresponds to the peak potential vorticity advection in the region (Fig. 14a). In NOPV, although areal coverage of precipitation remains similar, rain rates increase earlier, reflecting the earlier occurrence of potential vorticity advection as the northern anomaly extends southeastward. In NOPV, the reduced synoptic ascent, although producing less cirrus as expected (Fig. 18a), was still sufficient to promote convection. In 2XPV, the timing of the highest rain rates is similar to CNTL, although these peak rates persist longer. In addition, the areal coverage of precipitation increases by a factor of 5, with nearly 25% of the grid points within the 216 km by 216 km boxes centered on HBR and OKC producing precipitation by 0300 UTC (Fig. 17). This result reflects the importance of the synoptic forcing provided by the strengthened southern

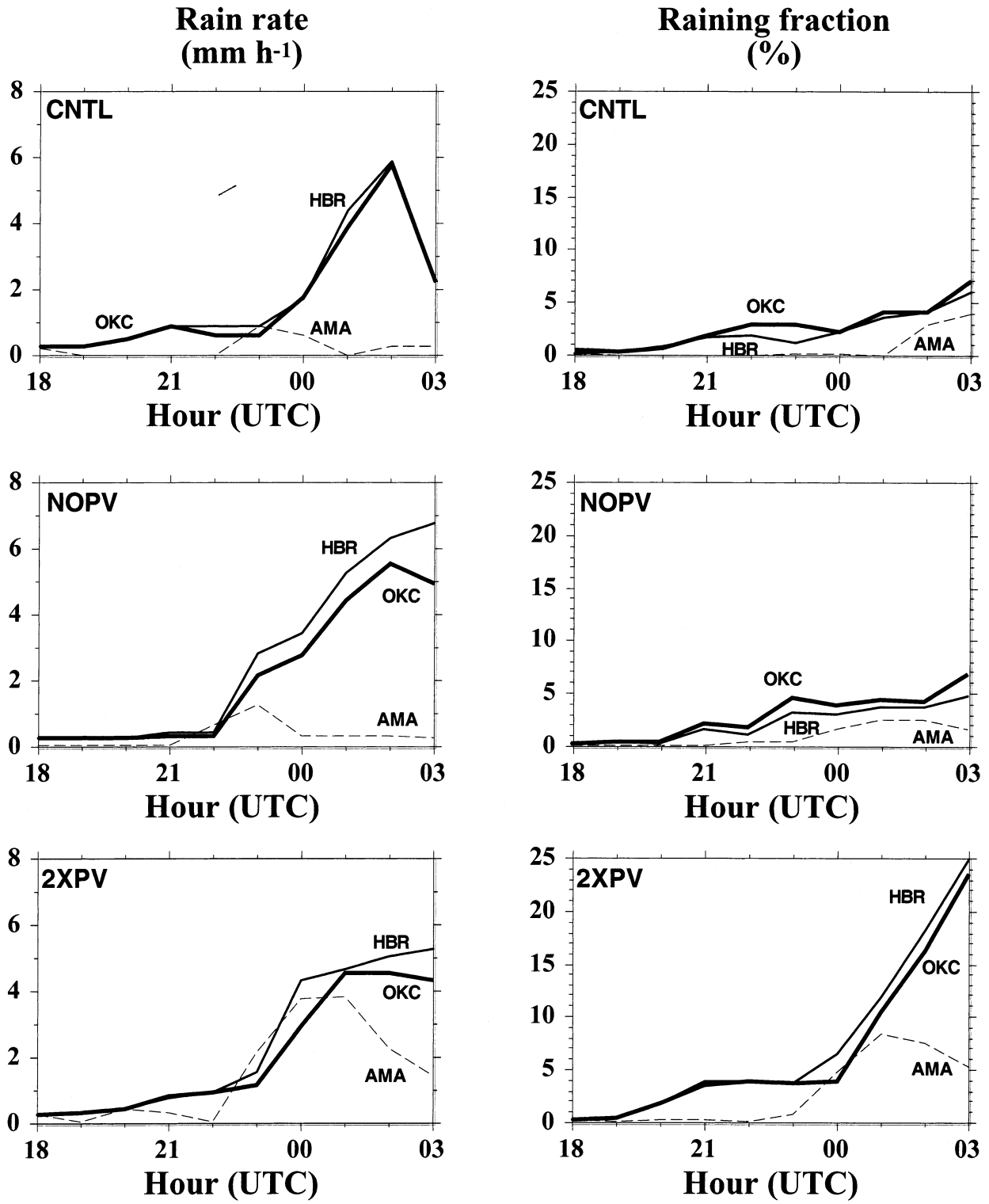


FIG. 17. Time series of hourly rainfall rate (mm $h^{-1}$) and raining fraction for 1800 UTC 3 May–0300 UTC 4 May 1999 for CNTL, NOPV, and 2XPV. Measures are computed within 216 km by 216 km boxes centered on grid points corresponding to the positions of AMA (dashed), HBR (solid), and OKC (thick solid; see Fig. 6 for site locations). Rainfall rate is averaged only for those grid points in which precipitation is occurring, whereas the raining fraction is defined by the percentage of grid points in which precipitation is occurring.

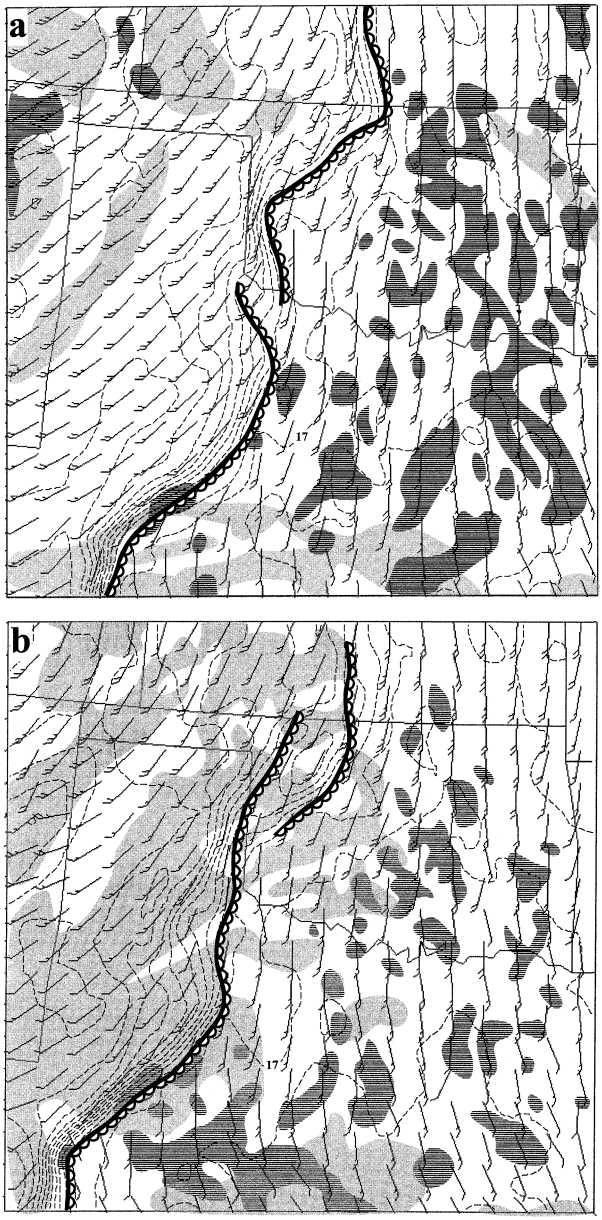


FIG. 18. (a) NOPV and (b) 2XPV 6-km grid-spacing domain (D3), valid at 2100 UTC 3 May 1999, showing vertically averaged cloud-water mixing ratio greater than 0.1 g kg$^{-1}$ (hatched), vertically averaged cloud-ice mixing ratio greater than 0.1 g kg$^{-1}$ (shaded), lowest sigma-level isodrosotherms (dashed lines every 2°C; 17°C contour labeled), and lowest sigma-level winds (as in Fig. 3). The dryline position is defined by the leading edge of the dewpoint temperature gradient greater than or equal to 15°C (100 km)$^{-1}$.

anomaly in promoting convective initiation, despite the existence of increased cirrus cloud (Fig. 18b).

These precipitation characteristics suggest that the details of storm structure may also vary between the simulations. Indeed, application of the supercell criterion of section 3d to 2XPV results in only five identifiable supercells, with maximum storm lifetimes and track lengths of 120 min and 125 km, respectively. In general, the supercells in 2XPV were short lived, and the convective evolution trended toward linear formations by the end of the run at 0300 UTC. The NOPV simulation, in which the BRNSHR and SRH values are similar to CNTL and correspondingly supportive of supercellular organization (Fig. 15), interestingly produces only four supercells. Unlike 2XPV, convective activity overall (as measured by the total number of updrafts exceeding 5 m s$^{-1}$) is reduced by 24% in NOPV relative to CNTL. This reduction in activity is likely tied to the weaker synoptic forcing in NOPV noted above. Three of the NOPV supercell storms, however, track through central Oklahoma, with one storm persisting to the end of the simulation at 0300 UTC, after covering 154 km in 210 min (Fig. 19). It may be that these robust supercells evolve in central Oklahoma in response to an environment in which overall storm competition is considerably reduced. Although each of the three simulations produced supercells, the character of the event was markedly different in each case, indicating the critical roles of the southern anomaly in regulating the event.

Given the paucity of upper-level observations, it is difficult to establish which of the three simulations (CNTL, NOPV, 2XPV) provides the most realistic representation of tropopause-level dynamics on 3 May 1999. Profiler observations at Purcell, a location ~60 km south of OKC, provide some indication of the evolution on that day (Fig. 20). BRNSHR increased rapidly at Purcell after 1800 UTC, reaching 173 m$^2$ s$^{-2}$ by 0200 UTC 4 May. Model gridpoint BRNSHR values in CNTL, NOPV, and 2XPV also show this growth. The trends in model BRNSHR show that the southern anomaly was mostly a negative influence on deep-layer shear, with 2XPV remaining well below NOPV through 0300 UTC 4 May at Purcell. CNTL and NOPV provide the closest match to the observed values at Purcell, although there are important differences between these runs and the observed values.

Some information on the spatial structure of the dynamic tropopause at 0000–0300 UTC 4 May 1999 is obtainable from the 0–3-h tropopause forecasts presented in Fig. 4. The southern anomaly was shown to interfere, in proportion to its magnitude, with the southeastward extension of the northern anomaly (cf. Figs. 3d, 12d, 13d). Because in nature, the southern anomaly and associated advections may have been somewhat weaker than depicted in CNTL (cf. Figs. 3d, 4b), the observed convection in central Oklahoma may have been linked to advections associated with the northern anomaly. This speculation is supported by the 0300 UTC 4 May 1999 (3-h forecast) position of the northern anomaly (Fig. 4b). In this respect, NOPV most closely mimicked nature. The southern anomaly, however, appears to have been directly relevant to the observed severe convection in northern Texas, and in that respect CNTL provides the better forecast.

The observed character of the event, then, was not precisely like any of the simulations, but rather resem-

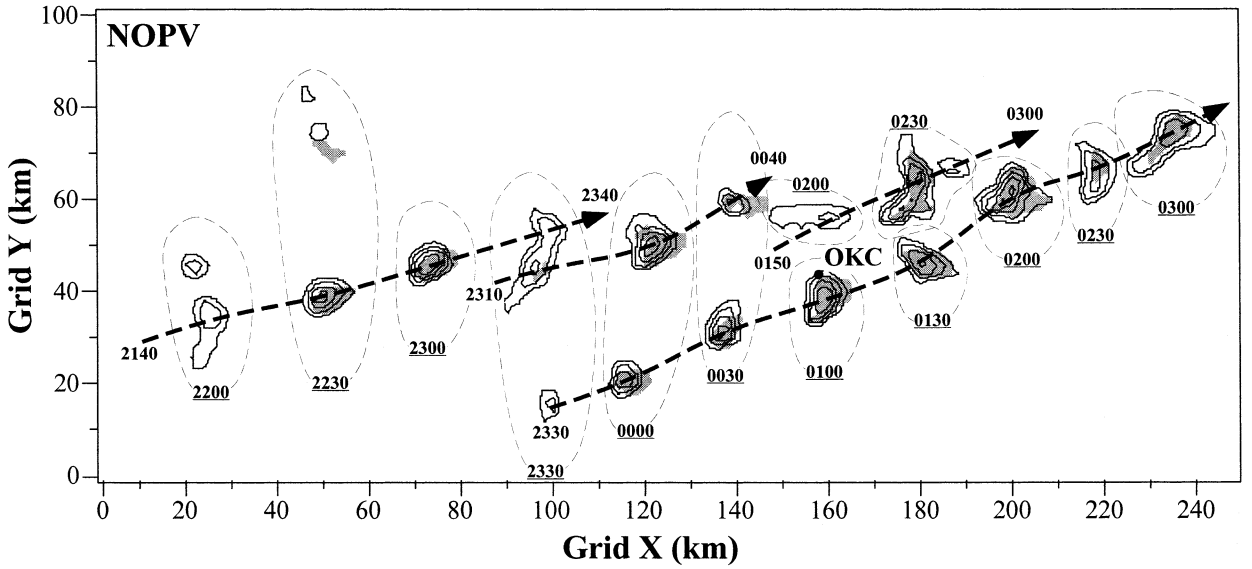


FIG. 19. NOPV storm histories for 2140 UTC 3 May–0300 UTC 4 May 1999 in central OK. Updrafts at height $z = 4$ km are shown by thin solid lines (contour interval of 6 m s$^{-1}$, first contour 6 m s$^{-1}$), vertical vorticity at $z = 4$ km exceeding $50 \times 10^{-4}$ s$^{-1}$ is enclosed by stippling, and the individual storm tracks are denoted by the dashed arrows (start and end times are indicated at the arrow start and end points, respectively). The thin dashed circle encloses equal times (UTC). Simulation end time is 0300 UTC 4 May 1999.

bled a compromise between the massive but mislocated outbreak scenario of CNTL and the intense, Oklahoma-centered supercells of NOPV. The 2XPV simulation, in this regard, is most useful in clarifying the dependence of the outbreak on the strength of the synoptic forcing. In particular, these findings support the speculation of TE that the outbreak would not have been as intense had numerous storms formed simultaneously in association with strong forcing. In 2XPV, the ascent associated with PV advections in advance of the artificially strengthened southern anomaly results in substantial convection, but with a trend toward linear storm structure, strikingly similar to the expectations in the 1246 UTC 3 May 1999 day-1 convective outlook (section 1).

### *c. Effects of the cirrus shield*

Given the possible importance of the cirrus to the inhibition of convective initiation when organized mesoscale boundaries are lacking, the removal of the southern anomaly might be expected to result in less cirrus and consequently more widespread convection. As shown in Fig. 18a, however, NOPV still has regions of cirrus present, associated with the PV advection from the northern anomaly (Figs. 12c,d, 14). To assess the direct role of the cirrus, we perform a fourth simulation, NOCR, in which the radiative effects of the clouds are switched off (i.e., from the point of view of the radiation budget, clouds do not exist in this simulation). In this way, the dynamic forcing of the southern anomaly is present, exactly as in CNTL, but without the confounding effects of the cirrus on the incoming solar radiation.

Storm interactions are next analyzed in CNTL and NOCR. Storm location is defined as the point in a $5 \times 5$ gridpoint box in D4 (64 km$^2$) at which the maximum updraft speed in the vertical is greater than or equal to 5 m s$^{-1}$. The minimum distance to the next updraft so defined is then computed, and these distance distributions are compiled at 10-min intervals from 1800 3 May to 0300 UTC 4 May 1999. The results of these calculations are plotted in a distance–time–frequency diagram (Fig. 21). In both simulations, the majority of the storms are closely spaced (<20 km apart). However, CNTL also shows a substantial number of isolated storms, with the number of such storms diminishing over time (Fig. 21a). This isolated storm activity is considerably reduced in NOCR (Fig. 21b), supporting the assertion that the cloud-radiative effects are important to storm organization in this case. Note that the updraft frequency is similar in the two runs through 2100 UTC; after this time, however, there is a sharp divergence, with peak activity nearly 7 times as great in NOCR as in CNTL during the period of 2230–0200 UTC (not shown). Hence, a primary role of the southern anomaly was to *limit the widespread development of convection* and subsequent storm interactions through the production of cirrus cloud while simultaneously *promoting convective initiation in focused areas* through weakening of the cap. As was shown above, the role of the southern anomaly in the production of deep-layer shear was decidedly nonlinear (Figs. 15, 20), the result of complex interactions between the southern anomaly and the approaching, stronger northern anomaly. The southern anomaly was mostly a negative influence on deep-layer shear, at least during the earliest stages of the event, because these interactions slowed the advance of the

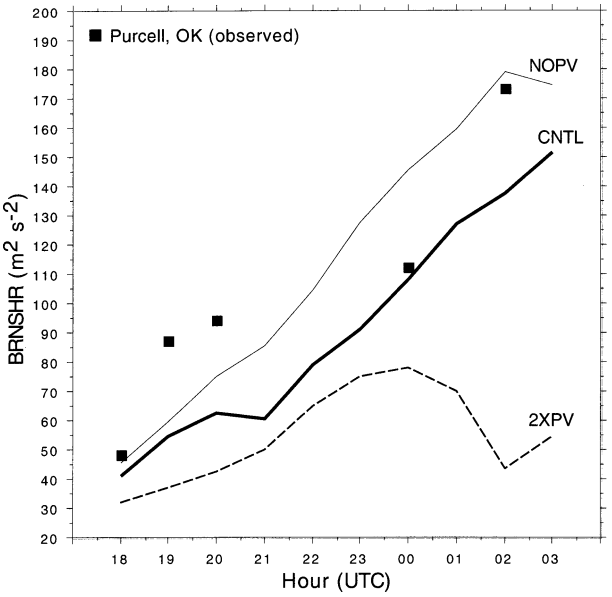


FIG. 20. Time series of BRNSHR ($m^2\ s^{-2}$) for 1800 UTC 3 May–0300 UTC 4 May 1999. Lines denote area-averaged values obtained for the 22 km × 22 km region centered at Purcell, OK, from the 2-km grid-spacing domain (D4) (thick line is CNTL, thin line is NOPV, and the dashed line is 2XPV). Also shown are observed values at Purcell (squares) for the times for which data are available (TE calculated the BRNSHR using the observed surface wind from an adjacent mesonet site, whereas these calculations use the profiler winds in total, without adjustment).

northern anomaly into the region. However, a key point is that the deep-layer shear would have been supportive of supercellular storms *independent of the existence of the southern anomaly.*

## 5. High-resolution models in operations: The hypothetical example of 3 May 1999

With the increasing use of mesoscale numerical models by researchers and forecasters in the 1980s, Keyser and Uccellini (1987) envisioned a fundamental change in how traditional synoptic studies would be conducted in both these communities. Now, mesoscale models have permeated both environments (e.g., Black 1994; Mass and Kuo 1998) and have advanced significantly in complexity and resolution. With this evolution in mesoscale modeling, the challenge of determining how to use their output effectively also increases (e.g., Brooks and Doswell 1993). This can best be understood in the context of the forecast process known as scientific forecasting.

### *a. Scientific forecasting: Hypothesis formation, hypothesis testing, and prediction*

Scientific forecasting is conducted through the linked execution of hypothesis formation, hypothesis testing, and prediction (Doswell 1986b; Doswell and Maddox 1986; Hoffman 1991; Andra et al. 2002). Hypothesis formation demands the development of a conceptual understanding of the forecast scenario, achieved through a diagnosis of the atmosphere's current state [defined by Doswell and Maddox (1986) as ''the re-creation of a coherent whole from those component parts considered during analysis; that is, a synthesis'']. Hypothesis testing requires seeking evidence (the nature of which will depend on the specific weather scenario and associated hypotheses) to support or refute the hypothesis. With the advent of NWP, this evidence is not solely observational; output from single or multiple NWP models may provide additional evidence to be used in the evaluation of the hypothesis. Because evidence in the form of observations or NWP model data may both be imperfect, several outcomes are possible. If the evidence supports the hypothesis, one may proceed to prediction with increased confidence. If the evidence refutes the hypothesis, however, the forecaster must decide whether the hypothesis requires revision or the evidence itself is flawed. In this way, an iterative process is achieved in which increased confidence in the forecast (and, it is hoped, convergence between the forecast and observations) can be attained.

The complexity of this process is increased with the use of NWP model output, for at least three reasons. First, it is generally less difficult to identify bad observational data than to recognize an incorrect model forecast ahead of time. Second, multiple model sources imply additional decisions in the usual circumstance in which the model solutions diverge. Third, skilled forecasters tend to examine ''subelements'' of NWP models rather than to use model output as intact representations of the atmospheric evolution (Pliske et al. 2002); this suggests that only portions of a model solution may be considered evidence at a given time.

Real-world operational constraints impose additional complications. Judgment and decision-making research has shown that as the amount of available information increases, the potential forecast skill increases at a faster rate than the skill actually achieved (Wright 1974; Heideman et al. 1993). Although actual skill may increase, the gains are modest relative to the resource investment (Heideman et al. 1993) and, in some cases, the accuracy of the forecasts may even decline (Stewart et al. 1992). Hence, improvements in forecasting might be obtained by devoting resources to improving the *use* of available information rather than necessarily increasing supply. When the latter occurs, however, improving the use of that information becomes even more important (Heideman et al. 1993). For example, Pliske et al. (2002) report that the U.S. Air Force (USAF) has made substantial investments in new technology (including mesoscale modeling) to support weather forecasting over the past decade in an attempt to minimize the impact of reductions in senior-level personnel. Despite this, USAF weather forecasting performance has declined (Pliske et al. 2002). Weather forecast technology design

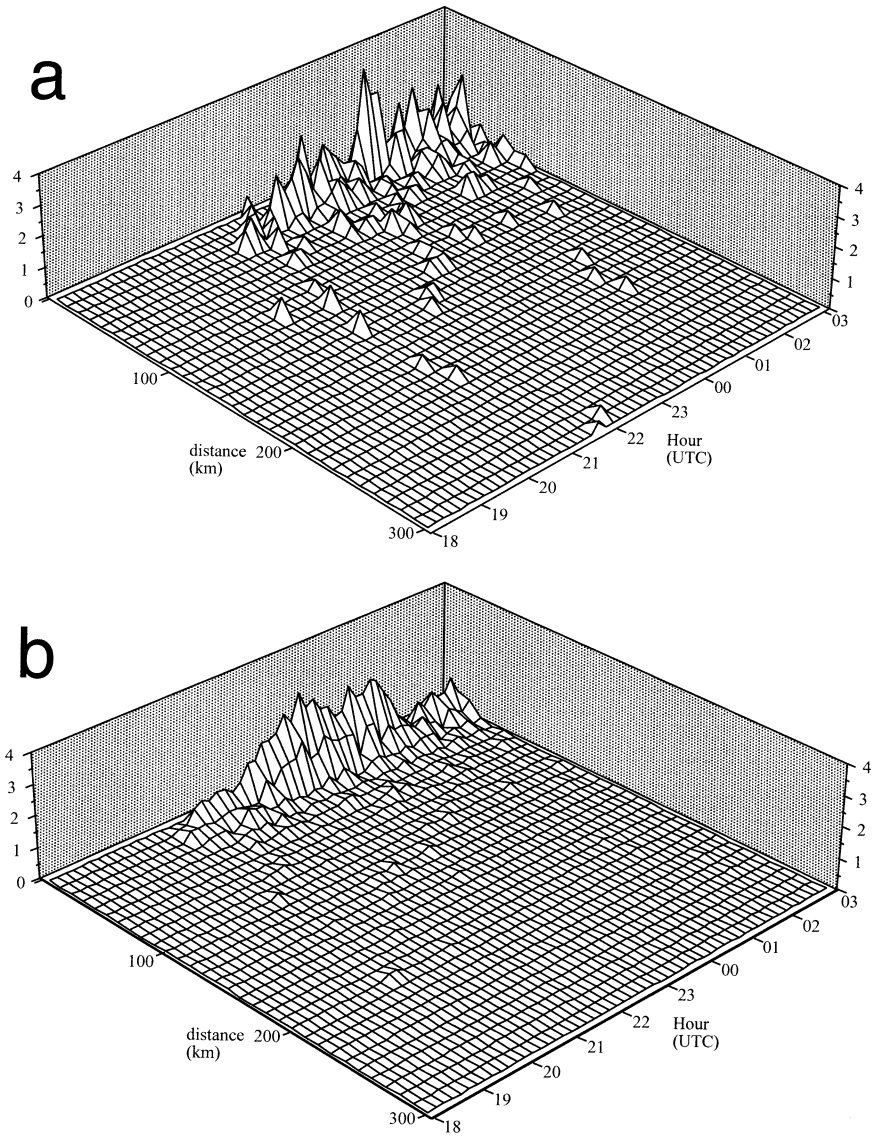


FIG. 21. Updraft distance–time–frequency diagram for maximum updrafts exceeding 5 m $s^{-1}$ in 2-km grid-spacing domain (D4) for 1800 UTC 3 May 1999–0300 UTC 4 May 1999. The vertical axis represents relative frequency for the entire period (i.e., normalized by the total number of updrafts). Shown are (a) CNTL and (b) NOCR.

considerations are also of considerable importance, because this can determine whether information, regardless of its value and the expertise of its users, can be effectively absorbed into operational practice (e.g., Hoffman 1991). Computational constraints are also a serious issue. It is certain that real-time forecasts of the kind produced in this paper are not easily achievable today (each simulation in this study required 5 h of clock time on a 24-processor workstation cluster). Nonetheless, the trends for the past 10 years in desktop machines suggest that this constraint will be eliminated by future computational advances.

One important consequence of applying scientific forecasting in the operational environment is that both quantitative and qualitative knowledge can be used throughout the forecast process; in this sense, the process is not objective. This ability to incorporate subjective information into a forecast can provide an advantage when forecasters are skilled in the forecast task—an assertion that is supported by the finding that the skill differential between experienced and novice forecasters is greatest for local forecast tasks (Roebber et al. 1996). This is further demonstrated by the observation that human forecasters have consistently outperformed objective forecasts of sensible weather (Olson et al. 1995) and that this skill advantage can translate into substantial additional value for some forecast applications (Roebber and Bosart 1996).

*b. Application to 3 May 1999*

The inability to incorporate subjective information into a forecast is perhaps most limiting in the case in which processes that influence the observations of eventual forecast interest are inadequately sampled. On 3 May 1999, one such process was the southern anomaly, which was poorly sampled owing to its offshore location yet had considerable influence on the evolution of the objective forecasts (section 4). As noted in section 1, there were many issues concerning convective initiation and mode about which the national-level SPC and local NWS forecasters were uncertain. How might high-resolution model output, such as that explored in this paper, have provided assistance to forecasters in their conduct of the scientific forecast process on 3 May 1999?

In the first stage of the forecast process, hypothesis formation, it was apparent that a favorable environment for severe convection would exist in the region (section 1). Diagnosis using rawinsondes, WSR-88D VWP wind profiles, and ACARS observations indicated that upper-level winds were likely to be stronger than forecast by the operational guidance (section 1) and suggested the possibility of supercellular organization (section 1; Tables 1 and 2). The 3 May 1999 event, however, did not conform to the existing conceptual model of the synoptically evident severe weather outbreak, owing to its dependence upon weak and/or subtle mesoscale processes for convective initiation (TE; E02). Hence, the hypothesis that was formed at 1246 UTC 3 May by SPC forecasters posited late-afternoon convective development, with a transition from isolated supercells to a linear mesoscale convective system (section 1; Tables 1 and 2). In the stage of hypothesis testing, several lines of evidence were examined. Operational NWP model precipitation forecasts showed little run-to-run consistency in the outbreak area, which, combined with weak (observed and forecast) convergence along the dryline, contributed to much uncertainty regarding convective initiation (E02). For example, although the 0000 UTC 3 May run of the Eta Model developed extensive convection ahead of the dryline, it represented a substantial departure from prior runs and was difficult to defend conceptually, leading to its disregard (E02). These uncertainties were summarized by TE (696–697, italics are those of the original authors):

> The predominance of a supercell convective mode and lack of a squall line on 3 May 1999 *may* have been attributable to the lack of strong low-level convergence near the dryline(s). It is conceivable that the outbreak would not have materialized in such intense or prolific form had the convergence been stronger along a consolidated dryline, and had numerous storms formed simultaneously. . . . However, . . . that same lack of convergence in the area of the drylines suggested that supercells might *not develop at all.*

Hence, although there was evidence to support severe convection, the prospects for convective initiation were mixed, the information supporting supercellular organization was ambiguous until late, and no observational, conceptual, or NWP model evidence existed to support an outbreak scenario. These uncertainties delayed the upgrade of the categorical convective outlook from ''slight'' to ''moderate'' risk until 1630 UTC 3 May (E02). Observational evidence from the wind profiler network later in the afternoon (section 2b in TE) reinforced the notion that sufficient shear would exist to support supercellular organization, but the problem of convective initiation remained. As stated by E02: ''observational diagnosis and analysis became more important and were critical in identification of the evolution of the outbreak. Tornadic supercells ultimately developed earlier, were more numerous, and produced more significant tornadoes than anticipated.''

Analysis of the four MM5 forecasts (CNTL, NOPV, 2XPV, NOCR) examined in this paper (sections 3 and 4) provided the following lines of evidence: 1) convective initiation was favored east of the dryline position in areas of a weakened cap, achieved through both surface heating and synoptic-scale ascent associated with the southern anomaly; 2) supercellular organization was supported regardless of the analysis details of the southern anomaly, although weak-to-moderate forcing from this feature was most conductive to the production of long-lived supercells; 3) the cirrus shield was important in limiting widespread development of convection and reducing competition between storms; and 4) an outbreak scenario was possible, but along with the location of the resulting convection, was highly sensitive to the analysis details of the southern anomaly.

How might this model evidence have been used to revise the hypothesis? The MM5 evidence unequivocally supported the notion of severe convection initiating east of the dryline position. The severe convection would be in the form of multiple supercells. Sites of convective initiation would be in areas where ample CAPE existed and the cap was weakening, the latter delineated by areas with substantial insolation and/or PV advection. It is important to recognize, however, that without forecaster confidence in the model, such a substantial revision to the hypothesis could not be made. Forecasters require information about the performance characteristics of the model, such as an understanding of the model ''climatology'' and false-alarm rates for particular phenomena. How often does the model produce long-lived supercells? How often do such forecasts verify?

Although there is at present no such information for supercellular organization, research suggests that storm-scale forecast models may be capable of providing considerable insight regarding convective initiation and mode, for a variety of synoptic situations. In a recent study of warm-season convection in the Great Lakes region (Fowle 2001), all days during the period of 5 April through 20 September 1999 were examined using

WSR-88D data and mesoscale-model forecasts. The probability of detection of convective initiation within a 348 km by 528 km region for this set of days was 0.82–0.84 while false alarm rates were 0.00–0.06 at 0–48-h forecast range, yielding Kuipers skill scores [also known as the true skill statistic, with 0 and 1 representing no skill and perfect skill, respectively; see Wilks (1995)] of 0.75–0.84. Skill for the determination of convective mode (categorized as linear, multicell, or isolated) was 0.86–0.91 for this same period.

Given that the evidence provided by the simulations in this paper was available to and was not rejected by forecasters, how could data be collected to test a revised hypothesis? Here, the limitations of the modern observing system are revealed. Because of the lack of a dense observational network that provides frequent profiles of temperature and moisture (Feltz and Mecikalski 2002), evidence of a weakening cap could only be directly addressed by looking at changes in surface temperature. Although modification of 1200 UTC soundings in this way is often beneficial, the spatial sampling is sufficiently coarse to constrain the usefulness of this exercise. For example, in the case of 3 May, available soundings in the region of interest would include Norman, Oklahoma (northeast of convective initiation); Amarillo (west of convective initiation), Dallas–Fort Worth, Texas (south); and Dodge City, Kansas (northwest). Satellite soundings in clear air provide another source of this information, but with an approaching cirrus shield, data availability would have become a problem just as conditions were becoming most critical. The limited availability of vertical profiles of other key variables would constrain other tests. Although wind profiles obtained from WSR-88D and ACARS would have been (and were) useful for evaluating trends in vertical wind shear, these data sources do not provide a means to analyze the spatial structure of the dynamic tropopause. Without a diagnosis of PV advection or another similar measure, it would prove difficult to isolate the most likely zones of convective initiation.

Forecasters have become adept at using indirect diagnosis strategies. For example, one might infer the PV advection from the evolution of the cirrus shield (detected by satellite observations). The appearance of the expanding cirrus shield after 1500 UTC 3 May 1999 raised questions in the forecasters' minds about whether the cirrus was associated with upper-level ascent due to the southern anomaly/jet streak (so-called active cirrus) or whether the cirrus was resulting from advection of high-level moisture from the subtropics (so-called passive cirrus, possibly enhanced by wave-cloud activity downstream of the Sierra Madre of northern Mexico and southern New Mexico; R. Thompson 2001, personal communication). Making this distinction was of obvious importance because of the expected differences in evolution under each scenario.

The paucity of observational data relates directly to the issue of real-world operational constraints. As noted above, introduction of additional information does not guarantee forecast improvement. In particular, it seems likely that introduction of high-resolution model data such as were examined here, without the means to test and to verify the guidance across the range of relevant scales, will yield only modest improvements in forecast skill. High-resolution model data are rendered considerably less effective with insufficient observations to test hypotheses and, in a worst case scenario, have the potential to degrade forecasting by supplanting observational diagnosis [e.g., the Advanced Weather Interactive Processing System (AWIPS) has made it comparatively easy to analyze model atmospheres relative to disparate and incomplete observational datasets; see also Pliske et al. (2002)]. Furthermore, the considerable effort required to glean value from a high-resolution model in a research setting cannot be transplanted effectively into operations without sufficient forecaster education, so that the forecasters possess the scientific knowledge required to interrogate intelligently the model data (Doswell 1986b; Pliske et al. 2002) and without accompanying technology to support the rapid discovery and absorption of the model information (e.g., Hoffman 1991; Wickens and Hollands 2000, 293–336). These constraints must be addressed before the capabilities highlighted in this paper can be transferred from the research arena to operations.

## 6. Summary

The Pennsylvania State University–National Center for Atmospheric Research MM5 is used at 2-km grid spacing in forecast mode (using the operational AVN run for initial and lateral boundary conditions) to examine forecast uncertainties (convective initiation and mode and their relation to the dryline, a cirrus shield, and a southern PV anomaly/jet streak) in the 3 May 1999 southern plains tornado outbreak. This work revealed the following major points:

- convective initiation was favored east of the dryline position in areas of a weakened cap, achieved through both surface heating and synoptic-scale ascent associated with the southern anomaly;
- supercellular organization was supported regardless of the analysis details of the southern anomaly, although weak-to-moderate forcing from this feature was most conducive to the production of long-lived supercells and strong forcing resulted in a trend toward linear mesoscale convective systems; the location of the convection was sensitive to these details;
- the cirrus shield was important in limiting widespread development of convection and reducing competition between storms; and
- in principle, forecasters following the scientific forecast process could have employed the model information in a way that would have assisted them in revising conceptual ideas about the evolution of the

outbreak; however, substantial obstacles to operational implementation of such a tool remain, including lack of model context (e.g., information concerning model biases), insufficient real-time observations to assess effectively model prediction details from the synoptic to the mesoscale, inconsistent forecaster education, and inadequate technology to support rapid scientific discovery in an operational setting.

*Acknowledgments.* The authors thank the following people for their contributions to this work: Richard Thompson and Roger Edwards gave their insights into the 3 May 1999 outbreak and their permission to use their graphics in our Fig. 1; Michael Baldwin provided the precipitation data and plotting software that made Fig. 5a possible; Dave Andra, Harold Brooks, Patrick Burke, Stephen Corfidi, Charles Doswell, David Dowell, Kimberly Elmore, Victor Homar, Harald Richter, David Stensrud, Stephen Weiss, and Louis Wicker shared their insights on various topics with the authors. The two anonymous reviewers are also thanked for their efforts.

The first author's Mesoscale Circulations class (Daniel Aber, Anthony Buss, Jane Fairchild, Michael Fowle, Timothy Halbach, Russel Harrings, Jessica Miller, Martin Pulrang, James Sieveking Jr., Kelly Wink, James Wood) was involved in the analysis of a ''pilot'' model simulation. A large portion of this work was accomplished during the first author's sabbatical at NSSL/SPC in December of 2000. The use of computing time and resources, and system administration, during his stay is gratefully acknowledged. Computing time was also kindly provided by WeatherEye, Inc., of Minneapolis, Minnesota. The authors thank the Oklahoma Climate Survey for providing the Oklahoma Mesonet data. This work is funded by NSF Grant OCE-9726679-03 and UCAR/COMET Grant SOO-18116.

## REFERENCES

Andra, D. L., Jr., E. M. Quoetone, and W. F. Bunting, 2002: Warning decision making: The relative roles of conceptual models, technology, strategy, and forecaster expertise on 3 May 1999. *Wea. Forecasting,* **17,** 559–566.

Anthes, R. A., 1986: The general question of predictability. *Mesoscale Meteorology and Forecasting,* P. S. Ray, Ed., Amer. Meteor. Soc., 636–656.

Atkins, N. T., M. L. Weisman, and L. J. Wicker, 1999: The influence of preexisting boundaries on supercell evolution. *Mon. Wea. Rev.,* **127,** 2910–2927.

Baldwin, M. E., and K. E. Mitchell, 1997: The NCEP hourly multisensor U.S. precipitation analysis for operations and GCIP research. Preprints, *13th Conf. on Hydrology,* Long Beach, CA, Amer. Meteor. Soc., 54–55.

Ballentine, R. J., A. J. Stamm, E. E. Chermack, G. P. Byrd, and D. Schleede, 1998: Mesoscale model simulation of the 4–5 January 1995 lake-effect snowstorm. *Wea. Forecasting,* **13,** 893–920.

Barnes, S. L., F. Caracena, and A. Marroquin, 1996: Extracting synoptic-scale diagnostic information from mesoscale models: The Eta model, gravity waves, and quasigeostrophic diagnostics. *Bull. Amer. Meteor. Soc.,* **77,** 519–528.

Bélair, S., D.-L. Zhang, and J. Mailhot, 1994: Numerical prediction of the 10–11 June 1985 squall line with the Canadian Regional Finite-Element Model. *Wea. Forecasting,* **9,** 157–172.

Black, T. L., 1994: The new NMC mesoscale Eta Model: Description and forecast examples. *Wea. Forecasting,* **9,** 265–278.

Blackadar, A. K., 1979: High resolution models of the planetary boundary layer. *Advances in Environmental Science and Engineering,* J. R. Pfafflin and E. N. Ziegler, Eds., Vol. 1, Gordon and Breach, 50–85.

Bluestein, H. B., 1993: *Observations and Theory of Weather Systems.* Vol. II. *Synoptic-Dynamic Meteorology in Midlatitudes,* Oxford University Press, 594 pp.

——, E. W. McCaul Jr., G. P. Byrd, and G. R. Woodall, 1988: Mobile sounding observations of a tornadic storm near the dryline: The Canadian, Texas storm of 7 May 1986. *Mon. Wea. Rev.,* **116,** 1790–1804.

Brooks, H. E., and C. A. Doswell III, 1993: New technology and numerical weather prediction—a wasted opportunity? *Weather,* **48,** 173–177.

——, and ——, 2001: Normalized damage from major tornadoes in the United States: 1890–1999. *Wea. Forecasting,* **16,** 168–176.

——, and ——, 2002: Deaths in the 3 May 1999 Oklahoma City tornado from a historical perspective. *Wea. Forecasting,* **17,** 354–361.

——, ——, and R. A. Maddox, 1992: On the use of mesoscale and cloud-scale models in operational forecasting. *Wea. Forecasting,* **7,** 120–132.

——, ——, and J. Cooper, 1994: On the environment of tornadic and nontornadic mesocyclones. *Wea. Forecasting,* **9,** 606–618.

Charney, J. G., 1955: The use of primitive equations of motion in numerical prediction. *Tellus,* **7,** 22–26.

Colle, B. A., and C. F. Mass, 2000: The 5–9 February 1996 flooding event over the Pacific Northwest: Sensitivity studies and evaluation of the MM5 precipitation forecasts. *Mon. Wea. Rev.,* **128,** 593–617.

——, K. J. Westrick, and C. F. Mass, 1999: Evaluation of MM5 and Eta-10 precipitation forecasts over the Pacific Northwest during the cool season. *Wea. Forecasting,* **14,** 137–154.

Davies-Jones, R. P., 1984: Streamwise vorticity: The origin of updraft rotation in supercell storms. *J. Atmos. Sci.,* **41,** 2991–3006.

Davis, C. A., and K. A. Emanuel, 1991: Potential vorticity diagnosis of cyclogenesis. *Mon. Wea. Rev.,* **119,** 1929–1953.

Doswell, C. A., III, 1986a: Short-range forecasting. *Mesoscale Meteorology and Forecasting,* P. S. Ray, Ed., Amer. Meteor. Soc., 689–719.

——, 1986b: The human element in weather forecasting. *Natl. Wea. Dig.,* **11,** 6–17.

——, 1987: The distinction between large-scale and mesoscale contribution to severe convection: A case study example. *Wea. Forecasting,* **2,** 3–16.

——, and R. A. Maddox, 1986: The role of diagnosis in weather forecasting. *Proc. 11th Conf. on Weather Forecasting and Analysis,* Kansas City, MO, Amer. Meteor. Soc., 177–182.

——, and E. N. Rasmussen, 1994: The effect of neglecting the virtual temperature correction on CAPE calculations. *Wea. Forecasting,* **9,** 625–629.

——, H. E. Brooks, and R. A. Maddox, 1996: Flash flood forecasting: An ingredients-based methodology. *Wea. Forecasting,* **11,** 560–581.

——, A. R. Moller, and H. E. Brooks, 1999: Storm spotting and public awareness since the first tornado forecasts of 1948. *Wea. Forecasting,* **14,** 544–557.

Droegemeier, K. K., S. M. Lazarus, and R. Davies-Jones, 1993: The influence of helicity on numerically simulated convective storms. *Mon. Wea. Rev.,* **121,** 2005–2029.

Dudhia, J., 1989: Numerical study of convection observed during the Winter Monsoon Experiment using a mesoscale two-dimensional model. *J. Atmos. Sci.,* **46,** 3077–3107.

——, 1993: A nonhydrostatic version of the Penn State–NCAR Me-

soscale Model: Validation tests and simulation of an Atlantic cyclone and cold front. *Mon. Wea. Rev.*, **121,** 1493–1513.
——, 1996: A multi-layer soil temperature model for MM5. Preprints, *Sixth Annual PSU/NCAR Mesoscale Model Users' Workshop*, Boulder, CO, National Center for Atmospheric Research, 49–50.
Edwards, R., S. F. Corfidi, R. L. Thompson, J. S. Evans, J. P. Craven, J. P. Racy, D. W. McCarthy, and M. D. Vescio, 2002: Storm Prediction Center forecasting issues related to the 3 May 1999 tornado outbreak. *Wea. Forecasting*, **17,** 544–558.
Feltz, W. F., and J. R. Mecikalski, 2002: Monitoring high temporal resolution convective stability indices using the ground-based Atmospheric Emitted Radiance Interferometer (AERI) during the 3 May 1999 Oklahoma–Kansas tornado outbreak. *Wea. Forecasting*, **17,** 445–455.
Fowle, M., 2001: Study of the convective forecast skill of very high resolution (6-km) NWP model data. M.S. thesis, Department of Mathematical Sciences, University of Wisconsin—Milwaukee, 93 pp. [Available from Department of Mathematical Sciences, University of Wisconsin—Milwaukee, Milwaukee, WI 53201-0413.]
Fulton, R. A., J. P. Breidenbach, D. J. Seo, D. A. Miller, and T. O'Bannon, 1998: The WSR-88D rainfall algorithm. *Wea. Forecasting*, **13,** 377–395.
Gall, R., and M. Shapiro, 2000: The influence of Carl-Gustaf Rossby on mesoscale weather prediction and an outlook for the future. *Bull. Amer. Meteor. Soc.*, **81,** 1507–1523.
Gallus, W. A., Jr., and M. Segal, 1999: Diabatic effects on late-winter cold front evolution: Conceptual and numerical model evaluations. *Mon. Wea. Rev.*, **127,** 1518–1537.
Grell, G. A., J. Dudhia, and D. R. Stauffer, 1994: A description of the Fifth-Generation Penn State/NCAR Mesoscale Model (MM5). NCAR Tech. Note NCAR/TN-398+STR, 138 pp. [Available from NCAR, P.O. Box 3000, Boulder, CO 80307-3000.]
Hakim, G. J., D. Keyser, and L. F. Bosart, 1996: The Ohio Valley wave-merger cyclogenesis event of 25–26 January 1978. Part II: Diagnosis using quasigeostrophic potential vorticity inversion. *Mon. Wea. Rev.*, **124,** 2176–2205.
Heideman, K. F., T. R. Stewart, W. R. Moninger, and P. Reagan-Cirincione, 1993: The Weather Information and Skill Experiment (WISE): The effect of varying levels of information on forecast skill. *Wea. Forecasting*, **8,** 25–36.
Hoffman, R. R., 1991: Human factors psychology in the support of forecasting: The design of advanced meteorological workstations. *Wea. Forecasting*, **6,** 98–110.
Hoskins, B. J., M. E. McIntyre, and A. W. Robertson, 1985: On the use and significance of isentropic potential vorticity maps. *Quart. J. Roy. Meteor. Soc.*, **111,** 877–946.
Huo, Z., D.-L. Zhang, and J. R. Gyakum, 1999a: Interaction of potential vorticity anomalies in extratropical cyclogenesis. Part I: Static piecewise inversion. *Mon. Wea. Rev.*, **127,** 2546–2561.
——, ——, and ——, 1999b: Interaction of potential vorticity anomalies in extratropical cyclogenesis. Part II: Sensitivity to initial perturbations. *Mon. Wea. Rev.*, **127,** 2563–2575.
Kain, J. S., and J. M. Fritsch, 1993: Convective parameterization for mesoscale models: The Kain–Fritsch scheme. *The Representation of Cumulus Convection in Numerical Models. Meteor. Monogr.*, No. 24, Amer. Meteor. Soc., 165–170.
Keyser, D., and L. W. Uccellini, 1987: Regional models: Research tools for synoptic meteorologists. *Bull. Amer. Meteor. Soc.*, **68,** 306–320.
Lackmann, G. M., 2002: Cold-frontal potential vorticity maxima, the low-level jet, and moisture transport in extratropical cyclones. *Mon. Wea. Rev.*, **130,** 59–74.
Lemon, L. R., and C. A. Doswell III, 1979: Severe thunderstorm evolution and mesocyclone structure as related to tornadogenesis. *Mon. Wea. Rev.*, **107,** 1184–1197.
Mass, C. F., and Y.-H. Kuo, 1998: Regional real-time numerical weather prediction: Current status and future potential. *Bull. Amer. Meteor. Soc.*, **79,** 253–263.
McCaul, E. W., Jr., and M. L. Weisman, 1996: Simulations of shallow supercell storms in landfalling hurricane environments. *Mon. Wea. Rev.*, **124,** 408–429.
Morgan, M. C., and J. W. Nielsen-Gammon, 1998: Using tropopause maps to diagnose midlatitude weather systems. *Mon. Wea. Rev.*, **126,** 2555–2579.
NCDC, 1999: *Storm Data.* Vol. 41, No. 5, 371 pp. [Available from National Climatic Data Center, 151 Patton Ave., Asheville, NC 28801.]
Olson, D. A., N. W. Junker, and B. Korty, 1995: Evaluation of 33 years of quantitative precipitation forecasting at the NMC. *Wea. Forecasting*, **10,** 498–511.
Petersen, R. A., and J. D. Stackpole, 1989: Overview of the NMC production suite. *Wea. Forecasting*, **4,** 313–322.
Pliske, R., B. Crandall, and G. Klein, 2002: Competence in weather forecasting. *Psychological Investigations of Competent Decision Making*, J. Shanteau, P. Johnson, and K. Smith, Eds., Cambridge University Press, in press.
Reisner, J., R. M. Rasmussen, and R. T. Bruintjes, 1998: Explicit forecasting of supercooled liquid water in winter storms using the MM5 mesoscale model. *Quart. J. Roy. Meteor. Soc.*, **124B,** 1071–1108.
Roebber, P. J., and L. F. Bosart, 1996: The complex relationship between forecast skill and forecast value: A real-world analysis. *Wea. Forecasting*, **11,** 544–559.
——, and M. G. Gehring, 2000: Real-time prediction of the lake breeze on the western shore of Lake Michigan. *Wea. Forecasting*, **15,** 298–312.
——, and J. Eise, 2001: The 21 June 1997 flood: Storm-scale simulations and implications for operational forecasting. *Wea. Forecasting*, **16,** 197–218.
——, L. F. Bosart, and G. S. Forbes, 1996: Does distance from the forecast site affect skill? *Wea. Forecasting*, **11,** 582–589.
Romero, R., 2001: Sensitivity of a heavy-rain-producing western Mediterranean cyclone to embedded potential-vorticity anomalies. *Quart. J. Roy. Meteor. Soc.*, **127,** 2559–2597.
Rotunno, R., and J. B. Klemp, 1985: On the rotation and propagation of simulated supercell thunderstorms. *J. Atmos. Sci.*, **42,** 271–292.
Schultz, D. M., and C. A. Doswell III, 2000: Analyzing and forecasting Rocky Mountain lee cyclogenesis often associated with strong winds. *Wea. Forecasting*, **15,** 152–173.
Speheger, D. A., C. A. Doswell III, and G. J. Stumpf, 2002: The tornadoes of 3 May 1999: Event verification in central Oklahoma and related issues. *Wea. Forecasting*, **17,** 362–381.
Stensrud, D. J., J. V. Cortinas Jr., and H. E. Brooks, 1997: Discriminating between tornadic and nontornadic thunderstorms using mesoscale model output. *Wea. Forecasting*, **12,** 613–632.
Stewart, T. R., K. F. Heideman, W. R. Moninger, and P. Reagan-Cirincione, 1992: Effects of improved information on the components of skill in weather forecasting. *Organ. Behav. Hum. Decis. Processes*, **53,** 107–134.
Thompson, R. L., and R. Edwards, 2000: An overview of environmental conditions and forecast implications of the 3 May 1999 tornado outbreak. *Wea. Forecasting*, **15,** 682–699.
Vasiloff, S. V., E. A. Brandes, R. P. Davies-Jones, and P. S. Ray, 1986: An investigation of the transition from multicell to supercell storms. *J. Climate Appl. Meteor.*, **25,** 1022–1036.
Wandishin, M. S., S. L. Mullen, D. J. Stensrud, and H. E. Brooks, 2001: Evaluation of a short-range multimodel ensemble system. *Mon. Wea. Rev.*, **129,** 729–747.
Weisman, M. L., and J. B. Klemp, 1984: The structure and classification of numerically simulated convective storms in directionally varying wind shears. *Mon. Wea. Rev.*, **112,** 2479–2498.
——, and R. Rotunno, 2000: The use of vertical wind shear versus helicity in interpreting supercell dynamics. *J. Atmos. Sci.*, **57,** 1452–1472.

Wickens, C. D., and J. G. Hollands, 2000: *Engineering Psychology and Human Performance.* Prentice Hall, 573 pp.

Wilks, D. S., 1995: *Statistical Methods in the Atmospheric Sciences: An Introduction.* Academic Press, 500 pp.

Wood, V. T., R. A. Brown, and D. W. Burgess, 1996: Duration and movement of mesocyclones associated with southern Great Plains thunderstorms. *Mon. Wea. Rev.,* **124,** 97–101.

Wright, P., 1974: The harassed decision maker: Time pressures, distractions and the use of evidence. *J. Appl. Psychol.,* **59,** 555–561.

Zhang, D. L., and R. A. Anthes, 1982: A high-resolution model of the planetary boundary layer—Sensitivity tests and comparisons with SESAME-79 data. *J. Appl. Meteor.,* **21,** 1594–1609.

——, H.-R. Chang, N. L. Seaman, T. T. Warner, and J. M. Fritsch, 1986: A two-way interactive nesting procedure with variable terrain resolution. *Mon. Wea. Rev.,* **114,** 1330–1339.

Ziegler, C. L., T. J. Lee, and R. A. Pielke Sr., 1997: Convective initiation at the dryline: A modeling study. *Mon. Wea. Rev.,* **125,** 1001–1026.